



CERN-EP-2023-263
16 November 2023

Observation of abnormal suppression of $f_0(980)$ production in p–Pb collisions at $\sqrt{s_{NN}} = 5.02$ TeV

ALICE Collaboration*

Abstract

The dependence of $f_0(980)$ production on the final-state charged-particle multiplicity in p–Pb collisions at $\sqrt{s_{NN}} = 5.02$ TeV is reported. The production of $f_0(980)$ is measured with the ALICE detector via the $f_0(980) \rightarrow \pi^+ \pi^-$ decay channel in a midrapidity region of $-0.5 < y < 0$. Particle yield ratios of $f_0(980)$ to π and $K^*(892)^0$ are found to be decreasing with increasing charged-particle multiplicity. The magnitude of the suppression of the $f_0(980)/\pi$ and $f_0(980)/K^*(892)^0$ yield ratios is found to be dependent on the transverse momentum p_T , suggesting different mechanisms responsible for the measured effects. Furthermore, the nuclear modification factor Q_{pPb} of $f_0(980)$ is measured in various multiplicity ranges. The Q_{pPb} shows a strong suppression of the $f_0(980)$ production in the p_T region up to about 4 GeV/c. The results on the particle yield ratios and Q_{pPb} for $f_0(980)$ may help to understand the late hadronic phase in p–Pb collisions and the nature of the internal structure of $f_0(980)$ particle.

arXiv:2311.11786v1 [nucl-ex] 20 Nov 2023

1 Introduction

Light scalar mesons, whose spin and parity are zero and even, respectively, are of particular interest as their nature can be explained with an exotic structure [1]. Among them, a long-standing puzzle is related to the quark composition of the $f_0(980)$ particle [2–4]. The $f_0(980)$ is suggested to be either a conventional meson ($q\bar{q}$) [5], a compact tetraquark [6], or a $K\bar{K}$ molecule [7]. By comparing different observables in heavy-ion collisions with those in pp interactions, the structure of the $f_0(980)$ can be probed.

The theory of the strong interaction, quantum chromodynamics (QCD), predicts the formation of a state of strongly interacting matter, the so-called quark–gluon plasma (QGP), under the conditions of high temperature and high energy density reached in relativistic heavy-ion collisions. Many observations at the Large Hadron Collider (LHC) and the Relativistic Heavy Ion Collider (RHIC), such as collective flow [8–11] and jet quenching [12–14], which is also manifest in the suppression of the yield of high-momentum hadrons [15, 16] due to in-medium partonic energy loss, contribute to the understanding of the QGP properties [17, 18]. Specifically, the nuclear modification factors for different particle species, defined as the ratio of the transverse momentum (p_T) distributions measured in heavy-ion collisions to the corresponding yields in pp interactions scaled by the number of nucleon–nucleon collisions, show a strong modification of the p_T spectra in large collision systems due to the presence of the hot and dense QGP medium. However, the nuclear modification factors are measured to be close to unity in minimum bias (MB) proton–nucleus (pA) collisions for $p_T > 8$ GeV/c [19], indicating no substantial modification in pA collisions in the high p_T range.

Another effect observed in pp and pA collisions at the LHC is a multiplicity-dependent enhancement of the production of strange hadrons relative to hadrons composed of up and down quarks, which is usually referred to as “strangeness enhancement” [20]. The measurement of particle yield ratios of $f_0(980)$ to π and $K^*(892)^0$ can be helpful to examine whether the $f_0(980)$ yield is influenced by the strangeness enhancement, thus providing sensitivity to the strange quark content inside the $f_0(980)$ [21, 22]. Moreover, other features observed in heavy-ion collisions, such as the strong enhancement of the nuclear modification factors of baryons at intermediate p_T ($2 < p_T < 5$ GeV/c) [18, 23] compared to those of mesons and the baryon and meson grouping of the elliptic flow [24], show an apparent dependence on the number of constituent quarks (NCQ) [24], reflecting the formation of hadrons from the QGP via quark coalescence [23]. Hence, measurements of $f_0(980)$ production in systems where a QGP may be created can help to constrain the number of quarks forming the $f_0(980)$.

Short-lived resonances, such as $\rho(770)^0$ [25], $K^*(892)^0$ [26, 27], $\Sigma(1385)^\pm$ [28], and $\Lambda(1520)$ [29] as well as $f_0(980)$, are good probes to study the properties of the system that results from the hadronization of a QGP [30, 31]. In the late stage of the evolution of the system formed in heavy-ion collisions, there are two relevant temperatures and corresponding timescales: the chemical freeze-out, when the inelastic interactions among the constituents are expected to cease, and the later kinetic freeze-out, when all (elastic) interactions stop [32]. Since the time interval between the chemical and the kinetic freeze-outs of the system (~ 10 fm/c) is comparable with the lifetime of resonances [33, 34], their decay products can actively interact with the hadronic gas via rescattering whereas regeneration can occur from interactions between particle pairs in the hadron gas. These two processes are designated as hadronic interactions in this Letter. The hadronic interactions result in modifications of resonance yields. The modifications can be studied by comparing the yield of resonances with those of long-lived or ground-state particles [35]. Measurements of $\rho(770)^0/(\pi^+ + \pi^-)$ [25] and $K^*(892)^0/(K^+ + K^-)$ [26, 27] yield ratios are good examples to study the properties of the late hadronic phase after the chemical freeze-out. It is worth mentioning that the ratios of particles with the same strangeness can eliminate potential strangeness enhancement effects in the ratio. Recently, system-size-dependent modifications of particle yields are also observed in small collision systems [26, 27], suggesting that rescattering and regeneration may also occur in high-multiplicity pp and p–Pb collisions. These hadronic interactions depend on the

hadronic cross section of the decay products inside the hadronic medium, the lifetimes of the resonance, and the duration of the hadronic phase. The suppression of resonance yields in the hadronic gas can be explained by rescattering dominating over regeneration. In addition, the final states of resonances decaying to $\pi\pi$, such as $f_0(980)$, $\rho(770)^0$, and $f_2(1270)$, are affected by the same cross section of pions and the medium, while the amount of hadronic interactions differs due to different lifetimes of these resonances. In this context, measuring the modification of the $f_0(980)$ yield may contribute to further understanding of the late hadronic phase.

In this Letter, multiplicity-dependent measurements of $f_0(980)$ production in p–Pb collisions at center-of-mass energy per nucleon–nucleon collision $\sqrt{s_{NN}} = 5.02$ TeV are reported for the first time. The $f_0(980)$ is measured at midrapidity ($-0.5 < y < 0$) in $0 < p_T < 8$ GeV/ c for different multiplicity classes. In Sec. 2, the experimental setup is described, while the reconstruction of $f_0(980)$ and the relative corrections are explained in Sec. 3. The study of systematic uncertainties for the measurement is reported in Sec. 4. In Sec. 5, p_T spectra, particle yield ratios, the nuclear modification factors, and model comparisons are discussed. Finally, conclusions are outlined in Sec. 6.

2 Experimental setup

The sample of MB p–Pb collisions at $\sqrt{s_{NN}} = 5.02$ TeV used for the present analysis was recorded using the ALICE detector in 2016. Due to the different energies of the proton and lead beams, the center-of-mass reference system in p–Pb collisions is shifted in rapidity by $\Delta y_{\text{cms}} = 0.465$ along the direction of the proton beam. In the following, the convention that y stands for y_{cms} is used. The ALICE apparatus during the LHC Run 2 is described in detail in Ref. [36]. The present analysis is carried out using the following detectors: the V0 [37], the Zero Degree Calorimeters (ZDC) [38], the Inner Tracking System (ITS) [39], the Time Projection Chamber (TPC) [40], and the Time-Of-Flight (TOF) [41].

The V0 detector consists of two arrays of scintillators located on both sides of the interaction point (IP), denoted as V0A and V0C, each made of 32 plastic scintillator strips, covering the full azimuthal angle within the pseudorapidity intervals $2.8 < \eta < 5.1$ and $-3.7 < \eta < -1.7$, respectively. Minimum bias p–Pb collisions are selected online by requiring a signal in both V0A and V0C detectors in coincidence with the LHC bunch crossing. The total charge deposited in the V0A on the Pb-going side is utilized to define the multiplicity classes. The collected MB sample corresponds to an integrated luminosity of 0.3 nb^{-1} [42]. The ZDC detects nucleons emitted from the colliding nucleus by nuclear de-excitation processes or knocked out from wounded nucleons, the so-called “slow” nucleons. Two identical sets of ZDCs, each composed of a neutron (ZN) and a proton (ZP) calorimeter, are located at 112.5 m from the ALICE IP on both sides, covering very forward rapidity regions. The ZDC provides the least biased centrality selection in p–Pb collisions [43].

The primary vertex position is reconstructed using the measured track segments in the Silicon Pixel Detector (SPD) [44], the innermost two layers of the ITS. The primary vertex position along the beam direction (z_{vtx}) is required to be in $|z_{\text{vtx}}| < 10$ cm from the nominal interaction point ($z_{\text{vtx}} = 0$). The pileup is reduced by rejecting events with multiple reconstructed vertices with the additional requirement that the distance between the primary vertex and any additional reconstructed vertex is larger than 0.8 cm. In addition, an inconsistency between the number of track candidates in the ITS and clusters in the SPD is used to further reduce the pileup events [45]. After these selections, the probability of pileup events is expected to be about 0.1% in the MB sample [46]. Charged particles are reconstructed down to $p_T = 0.15$ GeV/ c in the pseudorapidity range $|\eta| < 0.9$ over the full azimuth with the TPC and the ITS detectors, which are located inside a large solenoidal magnet, providing a uniform magnetic field of 0.5 T directed along the beam axis. Particle identification (PID) can be performed with the TPC and TOF. The TPC measures specific ionization energy loss dE/dx of charged tracks to separate particle species. The TOF is used for PID by measuring the flight time of charged particles from the primary vertex to the

TOF.

3 Data analysis

The $f_0(980)$ resonances are reconstructed via the decay channel $f_0(980) \rightarrow \pi^+\pi^-$, for which the branching ratio is reported to be $\text{B.R.} = (46 \pm 6)\%$ [47]. The $f_0(980)$ candidates are built from pairs of charged tracks reconstructed in the ITS and TPC. The tracks are required to have $p_T > 0.15 \text{ GeV}/c$ and $|\eta| < 0.8$ for a uniform detector acceptance. The reconstructed tracks are required to satisfy the standard selection criteria, as reported in [48], to guarantee that only tracks with high quality are selected. To ensure good track momentum resolution, the reconstructed tracks are required to have crossed at least 70 readout pad rows (out of a maximum of 159) in the TPC and to have at least two associated hits in the ITS (out of a maximum of 6), with at least one in the SPD. Selection criteria, which are dependent on p_T , are applied to the distance of closest approach of the track to the primary vertex in the transverse (d_{xy}) and longitudinal (d_z) directions, requiring $|d_z| < 2 \text{ cm}$ and $|d_{xy}| < (0.0105 + 0.0350 \times p_T^{-1.1}) \text{ cm}$ (with p_T in GeV/c), respectively, to suppress contamination from secondary charged particles originating from weakly decaying hadrons and interactions with the material.

The identification of charged pions is performed using the combined information of the TPC and TOF. The difference between the measured ionization energy loss and the expected value from a Bethe–Bloch parameterization obtained by assuming the particle is a pion is required to be within two standard deviations for the pion identification in the TPC. The difference between the measured flight time of the particle and the expected flight time for a pion is required to be within three standard deviations for the particle to be identified as a pion in the TOF. Tracks not having a signal associated in the TOF are identified using only the dE/dx information from the TPC.

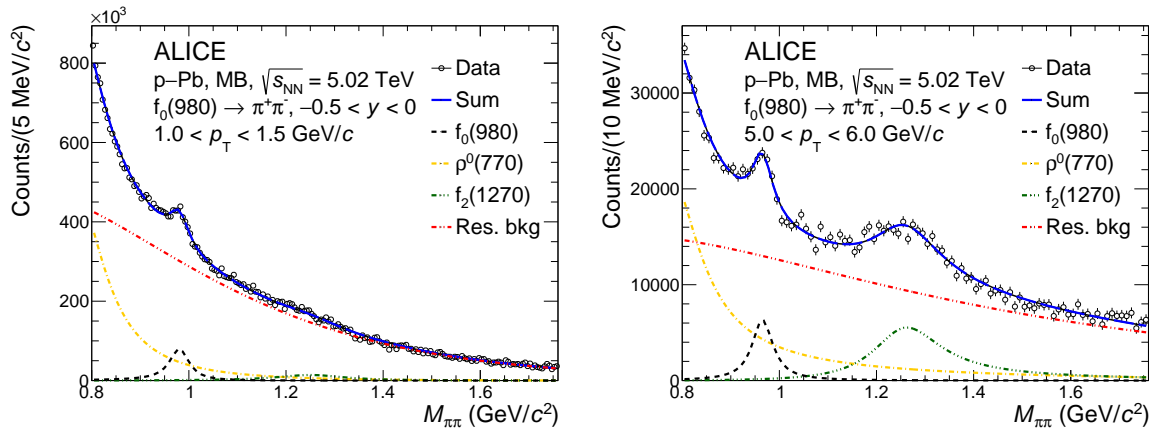


Figure 1: Invariant mass distribution of $\pi^+\pi^-$ pairs in $-0.5 < y < 0$ after the like-sign background subtraction in p–Pb collisions at $\sqrt{s_{\text{NN}}} = 5.02 \text{ TeV}$. The left (right) plot is obtained at low (high) p_T of $\pi^+\pi^-$ pairs in minimum bias events.

The $f_0(980)$ signals are extracted using an invariant mass analysis by associating two opposite-charge pions in the same event within $-0.5 < y < 0$ [49]. The combinatorial background is subtracted using the like-sign method [50]. The like-sign background is constructed as the geometric average of $\pi^+\pi^+$ and $\pi^-\pi^-$ distributions, $2\sqrt{N_{\pi^+\pi^+}N_{\pi^-\pi^-}}$. After subtracting the like-sign background from the $\pi^+\pi^-$ distribution, peaks of resonances decaying to $\pi^+\pi^-$ can be identified. Figure 1 shows the like-sign-subtracted $\pi^+\pi^-$ invariant mass ($M_{\pi\pi}$) distributions for $1.0 < p_T < 1.5 \text{ GeV}/c$ ($5.0 < p_T < 6.0 \text{ GeV}/c$) in MB events in the left (right) panel. Because $\rho(770)^0$ and $f_2(1270)$ dominantly decay to $\pi^+\pi^-$ and have large widths, $f_0(980)$ signals are overlapped with contributions from those two resonances. In addition, a residual background (f_{bkg}) is present, which is mainly attributed to misidentified particles and mini-jets. The measured invariant mass distribution is fitted with a function accounting for the contributions of

this residual background and of the three resonances. Each resonance contribution is described with a relativistic Breit-Wigner function (rBW) [25, 48]. Note that the detector resolution of $\mathcal{O}(1 \text{ MeV})$ gives a negligible contribution to the widths of broad resonances [27]. The rBW can be expressed as

$$\text{rBW}(M_{\pi\pi}) = \frac{AM_{\pi\pi}\Gamma(M_{\pi\pi})M_0}{(M_{\pi\pi}^2 - M_0^2)^2 + M_0^2\Gamma^2(M_{\pi\pi})}, \quad (1)$$

where $\Gamma(M_{\pi\pi})$ is defined as

$$\Gamma(M_{\pi\pi}) = \left[\frac{(M_{\pi\pi}^2 - 4m_\pi^2)}{(M_0^2 - 4m_\pi^2)} \right]^{(2J+1)/2} \times \frac{\Gamma_0 M_0}{M_{\pi\pi}}. \quad (2)$$

Here, A and M_0 are the amplitude of the rBW and the rest mass of the resonance, respectively. The rest width of the resonance, the spin, and the charged pion mass of $139.6 \text{ MeV}/c^2$ are represented as Γ_0 , J , and m_π , respectively. The spins for $f_0(980)$, $\rho(770)^0$, and $f_2(1270)$ are 0, 1, and 2, respectively. Each resonance rBW is corrected for the phase space factor [25], which can be expressed as

$$\text{PS}(M_{\pi\pi}) = \frac{M_{\pi\pi}}{\sqrt{M_{\pi\pi}^2 + p_T^2}} \times \exp(-\sqrt{M_{\pi\pi}^2 + p_T^2}/T_{\text{kin}}), \quad (3)$$

where p_T denotes the transverse momentum of the $\pi\pi$ pair and is set to be the median of each p_T interval, and T_{kin} is the kinetic freeze-out temperature, set to be 160 MeV [25] for all the defined multiplicity classes. The fit function for the background, f_{bkg} , is modeled with a Maxwell-Boltzmann-like distribution, which can be expressed as [51]

$$f_{\text{bkg}}(M_{\pi\pi}) = B(M_{\pi\pi} - 2m_\pi)^n \exp(c_1 M_{\pi\pi} + c_2 M_{\pi\pi}^2), \quad (4)$$

where, B , n , c_1 , and c_2 are free parameters.

The total fit function consists of the sum of three rBW's, one for each resonance and one function for the background, f_{bkg} . This function has nine free parameters: three for $f_0(980)$ resonance (mass, width, and amplitude), two amplitudes for $\rho(770)^0$ and $f_2(1270)$ resonances, and four parameters for f_{bkg} . In particular, the width of the $f_0(980)$ which is not yet constrained by measurements ($10 < \Gamma_0^{f_0} < 100 \text{ MeV}/c^2$ [1]) is left as a free parameter in the fit. The masses and widths of $\rho(770)^0$ and $f_2(1270)$ are fixed to their world-average values from Ref. [1], namely $m_\rho = 766.5 \text{ MeV}/c^2$, $\Gamma_0^\rho = 149.1 \text{ MeV}/c^2$, $m_{f_2} = 1,275.5 \text{ MeV}/c^2$, and $\Gamma_0^{f_2} = 186.7 \text{ MeV}/c^2$. Due to the many free parameters in the fit function, the procedure is split into three steps to prevent parameter values from converging to local minima. The purpose of the first step is to obtain an unbiased initial value for the $f_0(980)$ width. This step is performed using the MB sample over a coarse p_T binning to reduce the effect of statistical fluctuations. This coarse p_T binning is defined by merging 2 or 3 p_T bins of the finer p_T binning used for the analysis. All nine parameters are left free in the first step. The second step aims at constraining the f_{bkg} . The $f_0(980)$ width is fixed to the value determined from the wider p_T interval used in the previous step. The last step is processed fixing the parameters of f_{bkg} to those extracted in the previous step, while the $f_0(980)$ width is allowed to vary in the range of $10 < \Gamma_0^{f_0} < 100 \text{ MeV}/c^2$. In this procedure, the amplitudes of the three resonances and the mass of the $f_0(980)$ are left free, and the fit range is set to $0.8 < M_{\pi\pi} < 1.76 \text{ GeV}/c^2$. In the last step, the extracted width of $f_0(980)$ ranges between 40 and 70 MeV/c^2 in the different p_T and multiplicity intervals used in this analysis. The determination of the $f_0(980)$ width is sensitive to the modeling of the background and the other two resonances in the fit.

While for the $f_0(980)$ analysis performed in pp collisions [48], the width was constrained to be $55 \text{ MeV}/c^2$, the present analysis leaves the $f_0(980)$ width as a free parameter. In the previous analysis, no phase space correction was applied. On the other hand, the present analysis considers the phase space

correction for a possibly larger probability of $\pi\pi$ interference [52] owing to higher multiplicity in p–Pb collisions. It is found that consistent invariant yields in pp collisions are obtained from the two different analysis methods.

The raw yields of $f_0(980)$ (N_{f_0}) in each p_T interval are obtained by integrating the $f_0(980)$ rBW function. They are corrected for the acceptance, the tracking efficiency, and the PID efficiency and then normalized for the number of selected p–Pb collisions, the width of the p_T and rapidity interval, and the B.R. [47]. The fully corrected yield can be expressed as

$$\frac{1}{N_{\text{NSD}}} \frac{d^2N}{dydp_T} = \frac{1}{N_{\text{evt}}} \frac{N_{f_0}}{\Delta y \Delta p_T} \frac{\epsilon_{\text{trig}} f_{\text{vtx}} f_{\text{SL}}}{\text{Acc} \times \epsilon \times \text{B.R.}}. \quad (5)$$

Here, the number of events satisfying the event selection criteria in the specific multiplicity class is represented as N_{evt} . The corrected yield is then normalized to N_{NSD} , which is the number of non-single diffractive (NSD) events, via the factors $\epsilon_{\text{trig}} \times f_{\text{vtx}} \times f_{\text{SL}}$. The width of the rapidity interval (of 0.5 units) is represented as Δy . Coefficients for the acceptance (Acc) and the efficiency (ϵ) of the tracking and PID for pion pairs are estimated from a detailed simulation of the ALICE detector response. The p–Pb collisions are simulated using the DPMJET [53] event generator with the injection of $f_0(980)$ signals. The generated particles (signal and background) are transported through the detector using GEANT3 [54]. The $\text{Acc} \times \epsilon$ is estimated to be 26% in the $0 < p_T < 0.3$ GeV/ c interval and gradually increasing up to 60% as p_T increases, without any dependence on the multiplicity class. The B.R. is the branching ratio of the $f_0(980) \rightarrow \pi^+ \pi^-$ decay channel. The $f_0(980)$ yield is normalized for the trigger efficiency (ϵ_{trig}), vertex reconstruction efficiency (f_{vtx}), and signal loss (f_{SL}) due to the event selection. The ϵ_{trig} depends on the multiplicity class increasing from 0.84 to 1 as the multiplicity increases. The f_{vtx} is estimated to be larger than 0.99 in all measured multiplicity classes. The f_{SL} corrects for the $f_0(980)$ signal loss due to the event selection. Because general Monte Carlo event generators do not generate primary $f_0(980)$ particles, the f_{SL} is estimated using a different particle, the ϕ meson, exploiting the universal m_T scaling [55]. This approach shows that f_{SL} does not depend on particle species [34], and it is found to be 1.03 for $0 < p_T < 0.3$ GeV/ c and approaching unity for $p_T > 2$ GeV/ c .

4 Systematic uncertainties

The systematic uncertainties of the $f_0(980)$ yields are estimated by varying the analysis selection criteria, the configuration of the fit used to extract the raw yield, and the treatment of the phase space correction. The estimated uncertainties are summarized in Table 1. The total systematic uncertainty is calculated as the quadratic sum of the different contributing sources. The estimated uncertainties are different in the different multiplicity classes and the p_T intervals, but they do not show a clear trend as a function of multiplicity and p_T . In Table 1, the minimum and maximum uncertainty values are reported for each source. The relative uncertainty of the B.R. is 13% [47] and is not included in the total uncertainty.

The systematic uncertainty from the primary vertex selection is estimated by repeating the analysis with a different selection of $|z_{\text{vtx}}| < 7$ cm and found to be negligible. The systematic uncertainty from the pileup rejection is tested by varying the minimum number of track segments contributing to the reconstruction of pileup collision vertices from 5 to 3. The uncertainty is estimated to be negligible.

The systematic uncertainty from tracking is taken from [49], where uncertainties are evaluated by varying the requirements to select reconstructed primary tracks such as those on d_{xy} , d_z , and the number of crossed rows. The estimated uncertainty is 4%. The systematic uncertainty from the PID is tested with different requirements on the number of standard deviations ($\pm 0.5\sigma$ with respect to the default selections) for the TPC and TOF selection. The uncertainties are estimated to range from 4% to 12% in the different p_T intervals and multiplicity classes.

The uncertainties due to the $f_0(980)$ yield extraction via the fits to the invariant mass distributions are esti-

Table 1: Relative systematic uncertainties of the $f_0(980)$ p_T -differential yields. Numbers given in ranges correspond to minimum and maximum uncertainties.

Sources	Systematic uncertainty (%)
Primary vertex selection	negligible
Pileup rejection	negligible
Tracking	4
Particle identification	4–12
$f_2(1270)$ parameters	3–9
$\rho(770)^0$ parameters	3–8
Fit range	0–6
Initial f_0 width	2–12
Phase space correction	3–8
Total (in quadrature)	15–27

mated by varying some of the configurations in the fit procedure. The contributions coming from masses and widths of $f_2(1270)$ and $\rho(770)^0$ are evaluated by shifting the masses and the widths by three standard deviations with respect to their world-average values using the uncertainties reported in Ref. [1]. The estimated systematic uncertainties are 3–9% and 3–8%, respectively. Furthermore, the invariant mass range used in the fit is changed inward or outward by $40 \text{ MeV}/c^2$, and the resulting systematic uncertainty is found to be less than 6%. The contribution from the initial guess for the $f_0(980)$ width value, which is obtained in the first fit step described in Sec. 3, is estimated by varying the width within the statistical uncertainties, which is about $5 \text{ MeV}/c^2$ on average, in both directions. The variations affect the background distribution determined in the second step, and the estimated systematic uncertainties range from 2% to 12%. The systematic uncertainty from the phase space correction is estimated by varying the kinetic freeze-out temperature in the range of $140 < T_{\text{kin}} < 180 \text{ MeV}$. The estimated uncertainties range from 3% to 8%.

The correlations of the systematic uncertainties in different multiplicity classes are quantified. The uncertainty is considered more closely correlated when the directions of the systematic deviations are the same for different multiplicity classes. This is tested by comparing the directions of the systematic deviations between a given multiplicity class and the MB class. For all the sources of systematic uncertainty it is found that approximately half of the total systematic uncertainties are uncorrelated.

5 Results

Figure 2 shows the p_T spectra of $f_0(980)$ in p–Pb collisions at $\sqrt{s_{\text{NN}}} = 5.02 \text{ TeV}$ measured in the range of $0 < p_T < 8 \text{ GeV}/c$ for different multiplicity classes and NSD events. The multiplicity classes are defined based on the VOA amplitudes, which are proportional to the multiplicity of particles in the forward rapidity region of the Pb-going side. Each spectrum is scaled by a multiplicative factor denoted in the figure for visibility. The lower panel of Fig. 2 shows the ratios of the p_T spectra in different multiplicity classes to the NSD one. The systematic uncertainties of the ratios are estimated by propagating the multiplicity-uncorrelated uncertainties on the individual spectra. For $p_T < 4 \text{ GeV}/c$, a hardening of the p_T spectrum from low- to high-multiplicity events is clearly seen, while the spectral shapes in the different multiplicity classes are found to become consistent among each other for $p_T > 4 \text{ GeV}/c$. Such trends are similar to those observed for other hadronic species [15, 56] and are understood as due to the radial flow.

The integrated yield (dN/dy) and mean p_T ($\langle p_T \rangle$) of $f_0(980)$ are calculated by integrating and averaging the p_T spectrum, respectively. Table 2 shows the dN/dy and $\langle p_T \rangle$ of $f_0(980)$ for different multiplicity classes in p–Pb collisions at $\sqrt{s_{\text{NN}}} = 5.02 \text{ TeV}$. The dN/dy of $f_0(980)$ is found to increase linearly with charged-particle multiplicity when considering the $\langle dN_{\text{ch}}/d\eta \rangle$ values from Ref. [57], while the $\langle p_T \rangle$

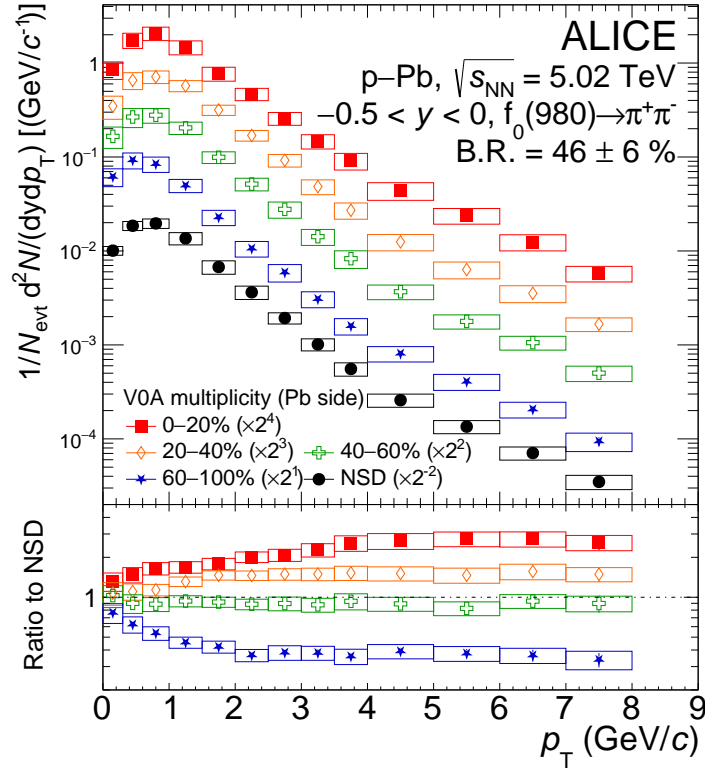


Figure 2: Transverse momentum spectra of $f_0(980)$ in p–Pb collisions at $\sqrt{s_{\text{NN}}} = 5.02$ TeV for different multiplicity classes, which are scaled for visibility. Statistical and systematic uncertainties are shown as error bars and boxes, respectively. The normalization uncertainty of 13% due to the uncertainty of the B.R. is not shown in the figure. The lower panel shows the ratios of the spectra in multiplicity classes to the NSD spectrum.

Table 2: The values of dN/dy and $\langle p_T \rangle$ for $f_0(980)$ measured in p–Pb collisions at $\sqrt{s_{\text{NN}}} = 5.02$ TeV for different multiplicity classes [57]. The first and second uncertainties represent the statistical and systematic uncertainties, respectively

Multiplicity class (VOA)	dN/dy	$\langle p_T \rangle$ (GeV/c)
0–20%	$0.206 \pm 0.005 \pm 0.014$	$1.287 \pm 0.034 \pm 0.010$
20–40%	$0.153 \pm 0.004 \pm 0.010$	$1.250 \pm 0.029 \pm 0.082$
40–60%	$0.113 \pm 0.002 \pm 0.008$	$1.142 \pm 0.025 \pm 0.088$
60–100%	$0.064 \pm 0.001 \pm 0.005$	$0.999 \pm 0.014 \pm 0.080$

exhibits a weak dependence on the charged-particle multiplicity.

The multiplicity dependence of $f_0(980)$ production is studied by comparing the ratio of the yields of different hadron species to that of pions in different multiplicity classes. A double ratio is calculated by dividing the hadron-to-pion yield ratios to their values measured in the lowest multiplicity interval, $(h/\pi)/(h/\pi)_{\text{LM}}$, allowing a direct comparison of multiplicity dependence among different hadron species and the reduction of the systematic uncertainties. The left panel of Fig. 3 shows the double ratios of different particles to charged pion yields as a function of charged-particle multiplicity raised to the power of 1/3 in p–Pb collisions at $\sqrt{s_{\text{NN}}} = 5.02$ TeV. The $\langle dN/d\eta \rangle_{|\eta| < 0.5}^{1/3}$ is a proxy for the size of the system [58]. The systematic uncertainty of the double ratio is calculated considering only the uncorrelated part of the uncertainty. The pion [19], $K^*(892)^0$ [27], and ϕ [27] mesons can be classified according to their lifetimes and to their (anti-)strange quark content. The strangeness enhancement and hadronic interactions can be studied by comparing the yield of particles with different characteristics. The double

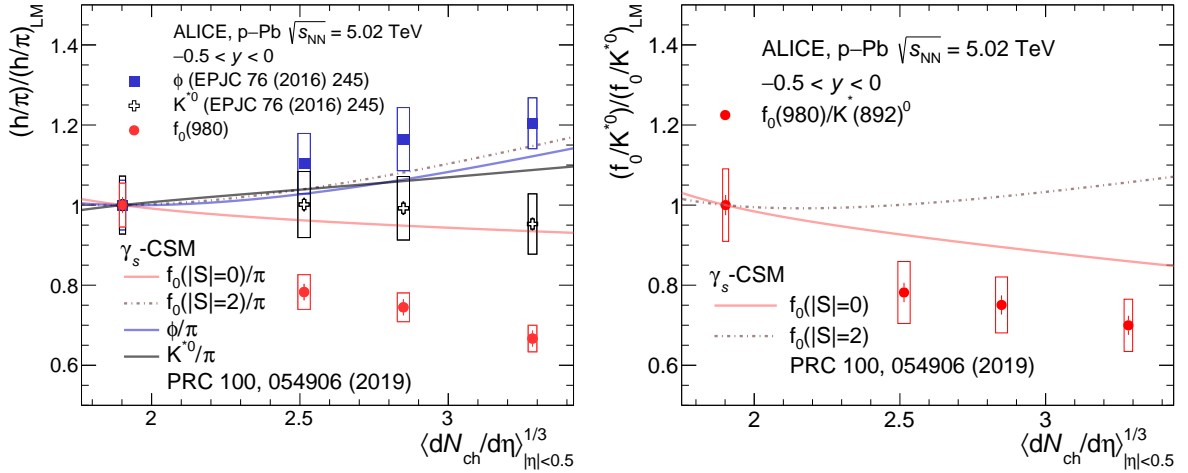


Figure 3: Double ratios of ϕ [27], $K^*(892)^0$ [27], and $f_0(980)$ to π [19] (left) and $f_0(980)$ to $K^*(892)^0$ (right) as a function of charged-particle multiplicity raised to the power of 1/3. The ratio in each multiplicity class is divided by the ratio in low-multiplicity (LM, 60–100%) events to allow for a direct comparison among different hadron species and reduce systematic uncertainties. V0A is utilized to categorize events based on their multiplicity. Predictions from the canonical statistical model are represented with lines.

ratio of ϕ to π increases with increasing multiplicity, which is consistent with the effect of the strangeness enhancement [20]. Due to the long lifetime (≈ 46.2 fm/c) of ϕ meson, little effect is expected from interactions in the hadronic phase. On the other hand, the double ratio of $K^*(892)^0$ to π is independent of multiplicity within the uncertainties even if $K^*(892)^0$ contains one strange quark. The flat trend could be explained by two competing effects, the strangeness enhancement and the interactions of the decay particles in the hadronic medium, due to the short lifetime (≈ 4.2 fm/c) of $K^*(892)^0$ [1]. One can expect that hadronic interactions reduce the $K^*(892)^0$ yield if the rescattering dominates over the regeneration. The double ratio of $f_0(980)$ to π decreases as the multiplicity increases because of the short lifetime (≈ 3 – 5 fm/c from the $\Gamma_0^{f_0}$ range estimated from our fits to the $f_0(980)$ line shape) of $f_0(980)$, suggesting that rescattering effects may play a role. Predictions of the ratio of $f_0(980)$ to π are shown in Fig. 3 (left) for different hidden strangeness ($|S|$) assumptions for $f_0(980)$ in the γ_s -Canonical Statistical Model (CSM) [59], where $|S|$ is the number of strange and anti-strange quarks. The CSM considers system-size-dependent hadrochemistry at vanishing baryon density with local conservation of electric charge, baryon density, and strangeness while allowing for undersaturation of strangeness. Note that γ_s is the parameter for the undersaturation of strangeness and is derived from a fit to the measured particle yields. The CSM hypothesis with two hidden strange quarks predicts an increase of the double ratio, contrary to what is observed experimentally. Moreover, the CSM with zero hidden strangeness predicts the $f_0(980)/\pi$ ratio to decrease much less than what is measured. When comparing the predicted trend to the measured one, it should however be considered that the CSM does not model interactions in the hadronic phase. The prediction of the CSM for the ϕ/π ratio qualitatively reproduces the increasing trend of the data with increasing multiplicity, where the hidden strangeness of ϕ is two. However, the CSM overestimates the ratio of $K^*(892)^0$ to π at high multiplicity because the modification of $K^*(892)^0$ yields due to rescattering effects is not implemented in the CSM, while the strangeness enhancement for $K^*(892)^0$ is included.

The right panel of Fig. 3 shows the double ratio of the $f_0(980)$ to $K^*(892)^0$ yield as a function of $\langle dN_{ch}/d\eta \rangle^{1/3}$ together with the predictions from the CSM with different hidden strangeness assumptions. The lifetimes of $f_0(980)$ and $K^*(892)^0$ are estimated to be of similar order of magnitude and both smaller than the duration of the hadronic phase in p–Pb collisions [1]. This leads to the expectation that the $f_0(980)/K^*(892)^0$ ratio is weakly affected by hadronic interactions, which depend on the hadronic cross section of the different decay products of the two resonances. The measured double ratio

shows a decreasing trend with increasing multiplicity, which is qualitatively described with the zero-hidden-strangeness assumption for $f_0(980)$ and can be explained by the strangeness enhancement of the $K^*(892)^0$ yield. The CSM prediction with the assumption of two hidden strange quarks is mildly increasing as the multiplicity increases, a trend that is opposite to the experimental result. The differences between the data point at the highest multiplicity and the two predictions with zero and two strange quarks amount to 2.3 and 5.2 standard deviations, calculated using the total uncertainty on the measurement, respectively. Therefore, the decreasing trend of the double ratio of $f_0(980)$ to $K^*(892)^0$ can suggest no effective strangeness enhancement for the $f_0(980)$. The discrepancies between the data and the model predictions can be attributed to the assumption of the same modification of $f_0(980)$ and $K^*(892)^0$ yields from hadronic interactions while the decay products from $f_0(980)$ and $K^*(892)^0$ differ.

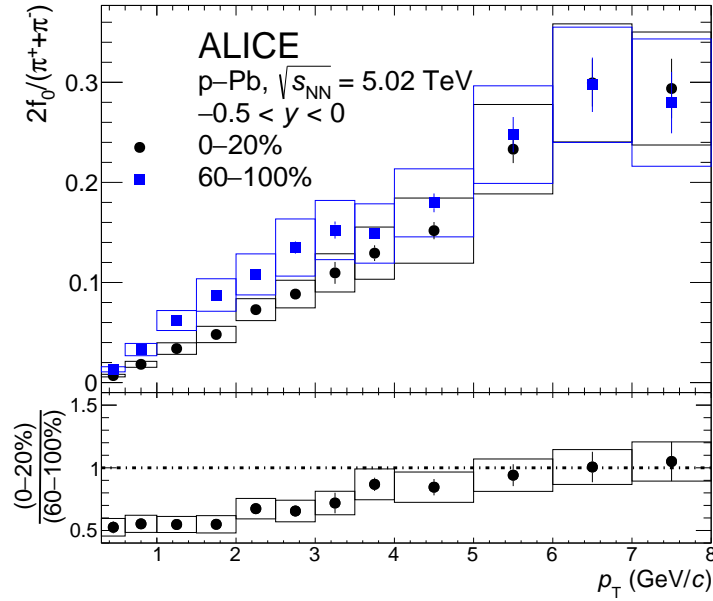


Figure 4: The particle yield ratios of $f_0(980)$ to π as a function of p_T in high-multiplicity (circles) and low-multiplicity (squares) p–Pb collisions at $\sqrt{s_{NN}} = 5.02$ TeV. The lower panel shows the double ratio of $f_0(980)/\pi$ between the high-multiplicity and low-multiplicity events. V0A is utilized to categorize events based on their multiplicity.

Figure 4 shows the p_T -differential particle yield ratio of $f_0(980)$ to π in high-multiplicity (HM, 0–20%) and low-multiplicity (LM, 60–100%) p–Pb collisions at $\sqrt{s_{NN}} = 5.02$ TeV. The ratios are consistent with each other within one sigma at $p_T > 4$ GeV/c, while at lower p_T the $f_0(980)$ to π ratio is systematically lower in the HM class as compared to the LM one. This suppression of $f_0(980)$ production at high multiplicity and low p_T is quantified via the double ratio reported in the lower panel of Fig. 4. In the double ratio, the correlated uncertainties across multiplicity classes cancel. The p_T dependence of the double ratio indicates that the suppression of the p_T -integrated yield shown in Fig. 3 is mainly occurring at low p_T values ($p_T < 3.5$ GeV/c), showing a qualitatively similar p_T dependence as the one reported in Ref. [26] for the suppression of the $K^*(892)^0/K$ ratios.

Figure 5 shows the p_T -differential particle yield ratio of $f_0(980)$ to $K^*(892)^0$ in HM and LM p–Pb collisions at $\sqrt{s_{NN}} = 5.02$ TeV. The ratio in HM events is lower than that in LM events in the entire p_T range, in contrast to what is observed for $K^*(892)^0/K$ and $f_0(980)/\pi$ ratios for which the suppression is observed only at low p_T . The suppression of the $f_0(980)/K^*(892)^0$ ratio in HM events for $p_T > 4$ GeV/c is evaluated to be 0.70 ± 0.04 (stat) ± 0.05 (syst) by fitting the double ratio with a constant function and indicates that other effects, beyond hadronic interactions, are present. For instance, the strangeness enhancement can explain the suppression of the $f_0(980)$ yield relative to that of $K^*(892)^0$ under the assumption that the $f_0(980)$ does not have strange quark content. This argument is also consistent with the decreasing

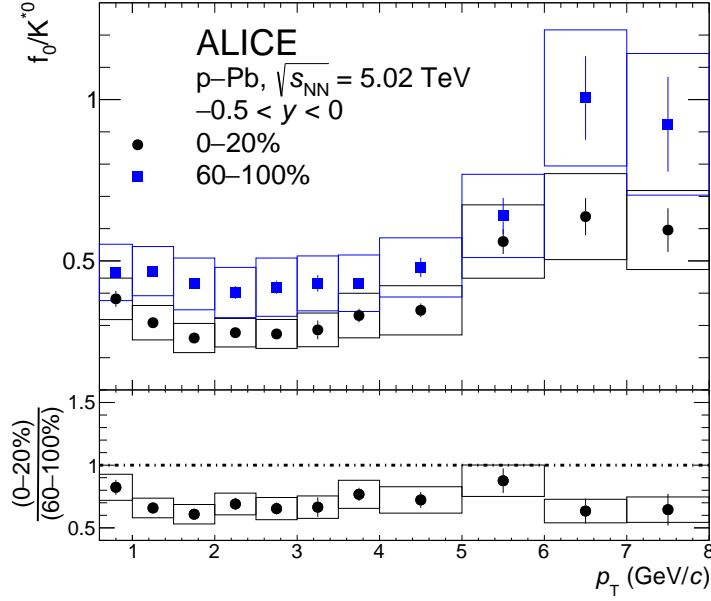


Figure 5: The particle yield ratio of $f_0(980)$ to $K^*(892)^0$ as a function of p_T in high-multiplicity (circles) and low-multiplicity (squares) p-Pb collisions at $\sqrt{s_{NN}} = 5.02$ TeV. The lower panel shows the double ratio of high-multiplicity to low-multiplicity $f_0(980)/K^*(892)^0$. V0A is utilized to categorize events based on their multiplicity.

trend of the p_T -integrated $f_0(980)/K^*(892)^0$ ratio with increasing multiplicity and their comparison to the CSM calculations shown in Fig. 3. In summary, the suppression of the $f_0(980)/K^*(892)^0$ ratio may suggest that the $f_0(980)$ does not contain strange quarks, and its production is therefore not affected by the strangeness enhancement. In addition, the enhancement of baryon-to-meson ratio at intermediate p_T , observed for p/ϕ , Λ/K_s^0 , Ξ/ϕ , and Ω/ϕ ratios [60], is not seen in the $f_0(980)/K^*(892)^0$ ratio, providing a hint that the number of constituent quarks for $f_0(980)$ is two.

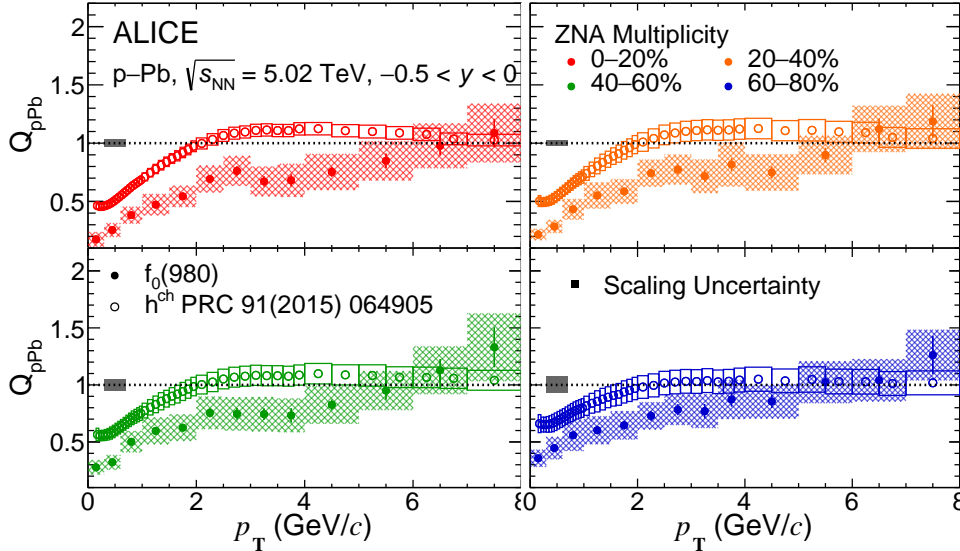


Figure 6: Nuclear modification factor (Q_{pPb}) of $f_0(980)$ as a function of p_T in p-Pb collisions at $\sqrt{s_{NN}} = 5.02$ TeV for different multiplicity classes. The multiplicity class is defined with the ZNA, which is the ZN placed on the Pb-going side. Statistical and systematic uncertainties are shown as error bars and boxes, respectively. Black boxes around unity represent the binary collision scaling uncertainties. The Q_{pPb} of charged hadrons [43] are reported for comparison.

The p_T -differential yield of $f_0(980)$ in p–Pb collisions can be compared to the one in pp collisions at the same center-of-mass energy by computing the nuclear modification factor Q_{pPb} , defined as

$$Q_{pPb} = \frac{d^2 N_{f_0(980)}^{pPb}/dp_T dy}{\langle T_{pPb} \rangle d^2 \sigma_{f_0(980)}^{pp}/dp_T dy}, \quad (6)$$

where $\langle T_{pPb} \rangle$ is the average nuclear overlap function, which is proportional to the number of binary nucleon–nucleon collisions, for the considered centrality class, and $d^2 \sigma_{f_0(980)}^{pp}/dp_T dy$ is the p_T differential cross section for $f_0(980)$ production in pp collisions taken from Ref. [48]. For this study, the centrality classes are defined using an event selection based on the ZN calorimeter in the Pb-going direction (ZNA) to minimize the possible selection biases, as reported in Ref [43].

Figure 6 shows the Q_{pPb} of $f_0(980)$ in p–Pb collisions at $\sqrt{s_{NN}} = 5.02$ TeV in different multiplicity classes. The systematic uncertainties are calculated with the assumption that there is no correlated uncertainty between the yield in pp and p–Pb collisions except for the B.R. uncertainty, which cancels out in the ratio. The scaling uncertainty on the Q_{pPb} shown in Fig. 6 is due to the uncertainty on $\langle T_{pPb} \rangle$, which is taken from Ref. [43]. The Q_{pPb} distributions of $f_0(980)$ are compared to those of charged hadrons [43]. At low p_T ($p_T < 4$ GeV/c), the Q_{pPb} of $f_0(980)$ is lower than unity indicating a suppression of the production in p–Pb collisions relative to pp collisions. This suppression becomes more pronounced with increasing multiplicity. Moreover, for $p_T < 4$ GeV/c the Q_{pPb} of $f_0(980)$ is also lower than that of charged hadrons and the difference increases with increasing multiplicity. As p_T increases, $f_0(980)$ Q_{pPb} values become compatible with those for charged particles, reaching unity. The dependencies of the nuclear modification factor on the multiplicity and p_T clearly indicate that rescattering largely contributes to the strong suppression of the $f_0(980)$ yield for $p_T < 4$ GeV/c. In addition, the Q_{pPb} does not exhibit a significant Cronin-like enhancement [61] at intermediate p_T in HM events. Since baryons show a more pronounced Cronin peak as compared to conventional mesons [19, 62], the absence of a significant Cronin-like enhancement of $f_0(980)$ might suggest that the $f_0(980)$ is composed of two quarks.

6 Conclusions

The multiplicity and p_T dependence of $f_0(980)$ production in p–Pb collisions at $\sqrt{s_{NN}} = 5.02$ TeV is presented. The $f_0(980)$ is reconstructed via the $f_0(980) \rightarrow \pi^+ \pi^-$ decay channel at midrapidity ($-0.5 < y < 0$) in the transverse momentum region of $0 < p_T < 8$ GeV/c. A hardening of the p_T spectra and a consequent increase of the mean p_T are observed with increasing multiplicity.

The p_T -integrated particle yield ratio of $f_0(980)$ to π decreases with increasing multiplicity, and the p_T -differential studies show a clear suppression of the $f_0(980)$ to π ratio for $p_T < 3.5$ GeV/c, indicating that rescattering effects for $f_0(980)$ particles exist in p–Pb collisions. The CSM overestimates the $f_0(980)/\pi$ ratio, and it does not describe the decreasing trend because the CSM does not consider rescattering processes. The p_T -integrated $f_0(980)/K^*(892)^0$ yield ratio also decreases with increasing multiplicity. The suppression of the $f_0(980)$ to $K^*(892)^0$ ratio is observed in the entire measured p_T range, showing a different p_T dependence relative to the one expected from a rescattering scenario. The CSM qualitatively describes the decreasing trend for the p_T -integrated $f_0(980)/K^*(892)^0$ ratio as a function of multiplicity with the assumption of no hidden strangeness for $f_0(980)$, while it overestimates the $f_0(980)/K^*(892)^0$ with the assumption of two strange quarks. These results indicate that the production of $K^*(892)^0$ is relatively enhanced compared with $f_0(980)$ due to the strangeness enhancement.

Additionally, the p_T -differential $f_0(980)/K^*(892)^0$ ratio does not exhibit the characteristic enhancement of baryon-to-meson ratios, suggesting a structure with two constituent quarks for the $f_0(980)$ resonance. Furthermore, the multiplicity-dependent nuclear modification factor (Q_{pPb}) for $f_0(980)$ exhibits a strong suppression at low p_T with a clear dependence on multiplicity, which can be explained by the rescattering

effects. In addition, no Cronin-like enhancement is observed in Q_{pPb} , even in high-multiplicity events. The absence of Cronin-like enhancement in the $f_0(980)$ may suggest that the $f_0(980)$ is composed of two quarks.

The abnormal suppression in terms of multiplicity and transverse momentum relative to other particles sheds light on the internal structure of $f_0(980)$ suggesting that it is a conventional meson with no hidden strange quarks and provides insight into the properties of the late hadronic phase in p–Pb collisions.

Acknowledgements

The ALICE Collaboration would like to thank all its engineers and technicians for their invaluable contributions to the construction of the experiment and the CERN accelerator teams for the outstanding performance of the LHC complex. The ALICE Collaboration gratefully acknowledges the resources and support provided by all Grid centres and the Worldwide LHC Computing Grid (WLCG) collaboration. The ALICE Collaboration acknowledges the following funding agencies for their support in building and running the ALICE detector: A. I. Alikhanyan National Science Laboratory (Yerevan Physics Institute) Foundation (ANSL), State Committee of Science and World Federation of Scientists (WFS), Armenia; Austrian Academy of Sciences, Austrian Science Fund (FWF): [M 2467-N36] and Nationalstiftung für Forschung, Technologie und Entwicklung, Austria; Ministry of Communications and High Technologies, National Nuclear Research Center, Azerbaijan; Conselho Nacional de Desenvolvimento Científico e Tecnológico (CNPq), Financiadora de Estudos e Projetos (Finep), Fundação de Amparo à Pesquisa do Estado de São Paulo (FAPESP) and Universidade Federal do Rio Grande do Sul (UFRGS), Brazil; Bulgarian Ministry of Education and Science, within the National Roadmap for Research Infrastructures 2020-2027 (object CERN), Bulgaria; Ministry of Education of China (MOEC), Ministry of Science & Technology of China (MSTC) and National Natural Science Foundation of China (NSFC), China; Ministry of Science and Education and Croatian Science Foundation, Croatia; Centro de Aplicaciones Tecnológicas y Desarrollo Nuclear (CEADEN), Cubaenergía, Cuba; Ministry of Education, Youth and Sports of the Czech Republic, Czech Republic; The Danish Council for Independent Research | Natural Sciences, the VILLUM FONDEN and Danish National Research Foundation (DNRF), Denmark; Helsinki Institute of Physics (HIP), Finland; Commissariat à l’Energie Atomique (CEA) and Institut National de Physique Nucléaire et de Physique des Particules (IN2P3) and Centre National de la Recherche Scientifique (CNRS), France; Bundesministerium für Bildung und Forschung (BMBF) and GSI Helmholtzzentrum für Schwerionenforschung GmbH, Germany; General Secretariat for Research and Technology, Ministry of Education, Research and Religions, Greece; National Research, Development and Innovation Office, Hungary; Department of Atomic Energy Government of India (DAE), Department of Science and Technology, Government of India (DST), University Grants Commission, Government of India (UGC) and Council of Scientific and Industrial Research (CSIR), India; National Research and Innovation Agency - BRIN, Indonesia; Istituto Nazionale di Fisica Nucleare (INFN), Italy; Japanese Ministry of Education, Culture, Sports, Science and Technology (MEXT) and Japan Society for the Promotion of Science (JSPS) KAKENHI, Japan; Consejo Nacional de Ciencia (CONACYT) y Tecnología, through Fondo de Cooperación Internacional en Ciencia y Tecnología (FONCICYT) and Dirección General de Asuntos del Personal Académico (DGAPA), Mexico; Nederlandse Organisatie voor Wetenschappelijk Onderzoek (NWO), Netherlands; The Research Council of Norway, Norway; Commission on Science and Technology for Sustainable Development in the South (COMSATS), Pakistan; Pontificia Universidad Católica del Perú, Peru; Ministry of Education and Science, National Science Centre and WUT ID-UB, Poland; Korea Institute of Science and Technology Information and National Research Foundation of Korea (NRF), Republic of Korea; Ministry of Education and Scientific Research, Institute of Atomic Physics, Ministry of Research and Innovation and Institute of Atomic Physics and Universitatea Nationala de Stiinta si Tehnologie Politehnica Bucuresti, Romania; Ministry of Education, Science, Research and Sport of the Slovak Republic, Slovakia; National Research Foundation of

South Africa, South Africa; Swedish Research Council (VR) and Knut & Alice Wallenberg Foundation (KAW), Sweden; European Organization for Nuclear Research, Switzerland; Suranaree University of Technology (SUT), National Science and Technology Development Agency (NSTDA) and National Science, Research and Innovation Fund (NSRF via PMU-B B05F650021), Thailand; National Academy of Sciences of Ukraine, Ukraine; Science and Technology Facilities Council (STFC), United Kingdom; National Science Foundation of the United States of America (NSF) and United States Department of Energy, Office of Nuclear Physics (DOE NP), United States of America. In addition, individual groups or members have received support from: European Research Council, Strong 2020 - Horizon 2020 (grant nos. 950692, 824093), European Union; Academy of Finland (Center of Excellence in Quark Matter) (grant nos. 346327, 346328), Finland.

References

- [1] **Particle Data Group** Collaboration, R. L. Workman *et al.*, “Review of Particle Physics”, *PTEP* **2022** (2022) 083C01.
- [2] **ExHIC** Collaboration, S. Cho *et al.*, “Multi-quark hadrons from Heavy Ion Collisions”, *Phys. Rev. Lett.* **106** (2011) 212001, arXiv:1011.0852 [nucl-th].
- [3] R. L. Jaffe, “Multi-Quark Hadrons. 1. The Phenomenology of (2 Quark 2 anti-Quark) Mesons”, *Phys. Rev. D* **15** (1977) 267.
- [4] L. Maiani, F. Piccinini, A. D. Polosa, and V. Riquer, “A New look at scalar mesons”, *Phys. Rev. Lett.* **93** (2004) 212002, arXiv:hep-ph/0407017.
- [5] C.-H. Chen, “Evidence for two quark content of $f_0(980)$ in exclusive $b \rightarrow c$ decays”, *Phys. Rev. D* **67** (2003) 094011, arXiv:hep-ph/0302059.
- [6] N. N. Achasov, J. V. Bennett, A. V. Kiselev, E. A. Kozyrev, and G. N. Shestakov, “Evidence of the four-quark nature of $f_0(980)$ and $f_0(500)$ ”, *Phys. Rev. D* **103** (2021) 014010, arXiv:2009.04191 [hep-ph].
- [7] H. A. Ahmed and C. W. Xiao, “Study the molecular nature of σ , $f_0(980)$, and $a_0(980)$ states”, *Phys. Rev. D* **101** (2020) 094034, arXiv:2001.08141 [hep-ph].
- [8] R. S. Bhalerao, “Collectivity in large and small systems formed in ultrarelativistic collisions”, *Eur. Phys. J. ST* **230** (2021) 635–654, arXiv:2009.09586 [nucl-th].
- [9] **ALICE** Collaboration, S. Acharya *et al.*, “Investigations of Anisotropic Flow Using Multiparticle Azimuthal Correlations in pp, p–Pb, Xe–Xe, and Pb–Pb Collisions at the LHC”, *Phys. Rev. Lett.* **123** (2019) 142301, arXiv:1903.01790 [nucl-ex].
- [10] **STAR** Collaboration, J. Adams *et al.*, “Experimental and theoretical challenges in the search for the quark gluon plasma: The STAR Collaboration’s critical assessment of the evidence from RHIC collisions”, *Nucl. Phys.* **A757** (2005) 102–183, arXiv:nucl-ex/0501009 [nucl-ex].
- [11] **PHENIX** Collaboration, K. Adcox *et al.*, “Formation of dense partonic matter in relativistic nucleus-nucleus collisions at RHIC: Experimental evaluation by the PHENIX collaboration”, *Nucl. Phys.* **A757** (2005) 184–283, arXiv:nucl-ex/0410003 [nucl-ex].
- [12] **ALICE** Collaboration, S. Acharya *et al.*, “Measurements of inclusive jet spectra in pp and central Pb–Pb collisions at $\sqrt{s_{NN}} = 5.02$ TeV”, *Phys. Rev. C* **101** (2020) 034911, arXiv:1909.09718 [nucl-ex].

- [13] **ATLAS** Collaboration, G. Aad *et al.*, “Observation of a Centrality-Dependent Dijet Asymmetry in Lead-Lead Collisions at $\sqrt{s_{\text{NN}}} = 2.77$ TeV with the ATLAS Detector at the LHC”, *Phys. Rev. Lett.* **105** (2010) 252303, arXiv:1011.6182 [hep-ex].
- [14] **PHENIX** Collaboration, A. Adare *et al.*, “Azimuthal anisotropy of neutral pion production in Au+Au collisions at $\sqrt{s_{\text{NN}}} = 200$ GeV: Path-length dependence of jet quenching and the role of initial geometry”, *Phys. Rev. Lett.* **105** (2010) 142301, arXiv:1006.3740 [nucl-ex].
- [15] **ALICE** Collaboration, S. Acharya *et al.*, “Production of charged pions, kaons, and (anti-)protons in Pb–Pb and inelastic pp collisions at $\sqrt{s_{\text{NN}}} = 5.02$ TeV”, *Phys. Rev. C* **101** (2020) 044907, arXiv:1910.07678 [nucl-ex].
- [16] **PHENIX** Collaboration, S. S. Adler *et al.*, “Common suppression pattern of η and π^0 mesons at high transverse momentum in Au+Au collisions at $\sqrt{s_{\text{NN}}} = 200$ GeV”, *Phys. Rev. Lett.* **96** (2006) 202301, arXiv:nucl-ex/0601037.
- [17] U. W. Heinz and M. Jacob, “Evidence for a new state of matter: An Assessment of the results from the CERN lead beam program”, arXiv:nucl-th/0002042.
- [18] **ALICE** Collaboration, “The ALICE experiment – A journey through QCD”, arXiv:2211.04384 [nucl-ex].
- [19] **ALICE** Collaboration, J. Adam *et al.*, “Multiplicity dependence of charged pion, kaon, and (anti)proton production at large transverse momentum in p–Pb collisions at $\sqrt{s_{\text{NN}}} = 5.02$ TeV”, *Phys. Lett. B* **760** (2016) 720–735, arXiv:1601.03658 [nucl-ex].
- [20] **ALICE** Collaboration, J. Adam *et al.*, “Enhanced production of multi-strange hadrons in high-multiplicity proton-proton collisions”, *Nature Phys.* **13** (2017) 535–539, arXiv:1606.07424 [nucl-ex].
- [21] **LHCb** Collaboration, R. Aaij *et al.*, “Measurement of resonant and CP components in $\bar{B}_s^0 \rightarrow J/\psi\pi^+\pi^-$ decays”, *Phys. Rev. D* **89** (2014) 092006, arXiv:1402.6248 [hep-ex].
- [22] **LHCb** Collaboration, R. Aaij *et al.*, “Measurement of the resonant and CP components in $\bar{B}^0 \rightarrow J/\psi\pi^+\pi^-$ decays”, *Phys. Rev. D* **90** (2014) 012003, arXiv:1404.5673 [hep-ex].
- [23] R. J. Fries, B. Muller, C. Nonaka, and S. A. Bass, “Hadronization in heavy ion collisions: Recombination and fragmentation of partons”, *Phys. Rev. Lett.* **90** (2003) 202303, arXiv:nucl-th/0301087.
- [24] M. Wang, J.-Q. Tao, H. Zheng, W.-C. Zhang, L.-L. Zhu, and A. Bonasera, “Number-of-constituent-quark scaling of elliptic flow: a quantitative study”, *Nucl. Sci. Tech.* **33** (2022) 37, arXiv:2203.10353 [hep-ph].
- [25] **ALICE** Collaboration, S. Acharya *et al.*, “Production of the $\rho(770)^0$ meson in pp and Pb–Pb collisions at $\sqrt{s_{\text{NN}}} = 2.76$ TeV”, *Phys. Rev. C* **99** (2019) 064901, arXiv:1805.04365 [nucl-ex].
- [26] **ALICE** Collaboration, S. Acharya *et al.*, “Multiplicity dependence of $K^*(892)^0$ and $\phi(1020)$ production in pp collisions at $\sqrt{s} = 13$ TeV”, *Phys. Lett. B* **807** (2020) 135501, arXiv:1910.14397 [nucl-ex].
- [27] **ALICE** Collaboration, J. Adam *et al.*, “Production of $K^*(892)^0$ and $\phi(1020)$ in p–Pb collisions at $\sqrt{s_{\text{NN}}} = 5.02$ TeV”, *Eur. Phys. J. C* **76** (2016) 245, arXiv:1601.07868 [nucl-ex].

- [28] ALICE Collaboration, S. Acharya *et al.*, “ $\Sigma(1385)^\pm$ resonance production in Pb–Pb collisions at $\sqrt{s_{\text{NN}}} = 5.02$ TeV”, *Eur. Phys. J. C* **83** (2023) 351, arXiv:2205.13998 [nucl-ex].
- [29] ALICE Collaboration, S. Acharya *et al.*, “Suppression of $\Lambda(1520)$ resonance production in central Pb–Pb collisions at $\sqrt{s_{\text{NN}}} = 2.76$ TeV”, *Phys. Rev. C* **99** (2019) 024905, arXiv:1805.04361 [nucl-ex].
- [30] C. Bierlich, T. Sjöstrand, and M. Uthm, “Hadronic rescattering in pA and AA collisions”, *Eur. Phys. J. A* **57** (2021) 227, arXiv:2103.09665 [hep-ph].
- [31] A. G. Knospe, C. Markert, K. Werner, J. Steinheimer, and M. Bleicher, “Hadronic resonance production and interaction in partonic and hadronic matter in the EPOS3 model with and without the hadronic afterburner UrQMD”, *Phys. Rev. C* **93** (2016) 014911, arXiv:1509.07895 [nucl-th].
- [32] C. Song and V. Koch, “Chemical relaxation time of pions in hot hadronic matter”, *Phys. Rev. C* **55** (1997) 3026–3037, arXiv:nucl-th/9611034.
- [33] ALICE Collaboration, K. Aamodt *et al.*, “Two-pion Bose-Einstein correlations in central Pb–Pb collisions at $\sqrt{s_{\text{NN}}} = 2.76$ TeV”, *Phys. Lett. B* **696** (2011) 328–337, arXiv:1012.4035 [nucl-ex].
- [34] ALICE Collaboration, S. Acharya *et al.*, “Evidence of rescattering effect in Pb–Pb collisions at the LHC through production of $K^*(892)^0$ and $\phi(1020)$ mesons”, *Phys. Lett. B* **802** (2020) 135225, arXiv:1910.14419 [nucl-ex].
- [35] ALICE Collaboration, S. Acharya *et al.*, “Multiplicity dependence of light-flavor hadron production in pp collisions at $\sqrt{s} = 7$ TeV”, *Phys. Rev. C* **99** (2019) 024906, arXiv:1807.11321 [nucl-ex].
- [36] ALICE Collaboration, B. B. Abelev *et al.*, “Performance of the ALICE Experiment at the CERN LHC”, *Int. J. Mod. Phys. A* **29** (2014) 1430044, arXiv:1402.4476 [nucl-ex].
- [37] ALICE Collaboration, E. Abbas *et al.*, “Performance of the ALICE VZERO system”, *JINST* **8** (2013) P10016, arXiv:1306.3130 [nucl-ex].
- [38] ALICE Collaboration, P. Cortese, “Performance of the ALICE Zero Degree Calorimeters and upgrade strategy”, *J. Phys. Conf. Ser.* **1162** (2019) 012006.
- [39] ALICE Collaboration, K. Aamodt *et al.*, “Alignment of the ALICE Inner Tracking System with cosmic-ray tracks”, *JINST* **5** (2010) P03003, arXiv:1001.0502 [physics.ins-det].
- [40] J. Alme *et al.*, “The ALICE TPC, a large 3-dimensional tracking device with fast readout for ultra-high multiplicity events”, *Nucl. Instrum. Meth. A* **622** (2010) 316–367, arXiv:1001.1950 [physics.ins-det].
- [41] ALICE Collaboration, N. Jacazio, “PID performance of the ALICE-TOF detector at Run 2”, *PoS LHCP2018* (2018) 232, arXiv:1809.00574 [physics.ins-det].
- [42] ALICE Collaboration, B. B. Abelev *et al.*, “Measurement of visible cross sections in proton-lead collisions at $\sqrt{s_{\text{NN}}} = 5.02$ TeV in van der Meer scans with the ALICE detector”, *JINST* **9** (2014) P11003, arXiv:1405.1849 [nucl-ex].
- [43] ALICE Collaboration, J. Adam *et al.*, “Centrality dependence of particle production in p–Pb collisions at $\sqrt{s_{\text{NN}}} = 5.02$ TeV”, *Phys. Rev. C* **91** (2015) 064905, arXiv:1412.6828 [nucl-ex].

- [44] R. Santoro *et al.*, “The ALICE Silicon Pixel Detector: Readiness for the first proton beam”, *JINST* **4** (2009) P03023.
- [45] ALICE Collaboration, J. Adam *et al.*, “Charged-particle multiplicities in proton–proton collisions at $\sqrt{s} = 0.9$ to 8 TeV”, *Eur. Phys. J. C* **77** (2017) 33, arXiv:1509.07541 [nucl-ex].
- [46] ALICE Collaboration, S. Acharya *et al.*, “Constraints on jet quenching in p–Pb collisions at $\sqrt{s_{NN}} = 5.02$ TeV measured by the event-activity dependence of semi-inclusive hadron-jet distributions”, *Phys. Lett. B* **783** (2018) 95–113, arXiv:1712.05603 [nucl-ex].
- [47] S. Stone and L. Zhang, “Use of $B \rightarrow J/\psi f_0$ decays to discern the $q\bar{q}$ or tetraquark nature of scalar mesons”, *Phys. Rev. Lett.* **111** (2013) 062001, arXiv:1305.6554 [hep-ex].
- [48] ALICE Collaboration, S. Acharya *et al.*, “ $f_0(980)$ production in inelastic pp collisions at $\sqrt{s} = 5.02$ TeV”, *Phys. Lett. B* **846** (2023) 137644, arXiv:2206.06216 [nucl-ex].
- [49] ALICE Collaboration, B. B. Abelev *et al.*, “Multiplicity Dependence of Pion, Kaon, Proton and Lambda Production in p–Pb Collisions at $\sqrt{s_{NN}} = 5.02$ TeV”, *Phys. Lett. B* **728** (2014) 25–38, arXiv:1307.6796 [nucl-ex].
- [50] T. Sjöstrand and M. van Zijl, “A multiple-interaction model for the event structure in hadron collisions”, *Phys. Rev. D* **36** (Oct, 1987) 2019–2041.
<https://link.aps.org/doi/10.1103/PhysRevD.36.2019>.
- [51] OPAL Collaboration, K. Ackerstaff *et al.*, “Photon and light meson production in hadronic Z^0 decays”, *Eur. Phys. J. C* **5** (1998) 411–437, arXiv:hep-ex/9805011.
- [52] STAR Collaboration, J. Adams *et al.*, “ p^0 production and possible modification in Au+Au and p+p collisions at $\sqrt{s_{NN}} = 200$ GeV”, *Phys. Rev. Lett.* **92** (2004) 092301, arXiv:nucl-ex/0307023.
- [53] A. Fedynitch, *Cascade equations and hadronic interactions at very high energies*. PhD thesis, KIT, Karlsruhe, Dept. Phys., 11, CERN-THESIS-2015-371.
- [54] R. Brun, F. Bruyant, F. Carminati, S. Giani, M. Maire, A. McPherson, G. Patrick, and L. Urban, “GEANT Detector Description and Simulation Tool”, *CERN-W5013* (10, 1994).
- [55] L. Altenkämper, F. Bock, C. Loizides, and N. Schmidt, “Applicability of transverse mass scaling in hadronic collisions at energies available at the CERN Large Hadron Collider”, *Phys. Rev. C* **96** (2017) 064907, arXiv:1710.01933 [hep-ph].
- [56] E. Schnedermann, J. Sollfrank, and U. W. Heinz, “Thermal phenomenology of hadrons from 200-A/GeV S+S collisions”, *Phys. Rev. C* **48** (1993) 2462–2475, arXiv:nucl-th/9307020.
- [57] ALICE Collaboration, B. Abelev *et al.*, “Pseudorapidity density of charged particles in p–Pb collisions at $\sqrt{s_{NN}} = 5.02$ TeV”, *Phys. Rev. Lett.* **110** (2013) 032301, arXiv:1210.3615 [nucl-ex].
- [58] P. Liu and R. A. Lacey, “System-size dependence of the viscous attenuation of anisotropic flow in p + Pb and Pb + Pb collisions at energies available at the CERN Large Hadron Collider”, *Phys. Rev. C* **98** (2018) 031901, arXiv:1804.04618 [nucl-ex].
- [59] V. Vovchenko, B. Dönigus, and H. Stoecker, “Canonical statistical model analysis of p-p, p–Pb, and Pb-Pb collisions at energies available at the CERN Large Hadron Collider”, *Phys. Rev. C* **100** (2019) 054906, arXiv:1906.03145 [hep-ph].















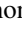




- [60] **ALICE** Collaboration, S. Acharya *et al.*, “Production of light-flavor hadrons in pp collisions at $\sqrt{s} = 7$ and $\sqrt{s} = 13$ TeV”, *Eur. Phys. J. C* **81** (2021) 256, arXiv:2005.11120 [nucl-ex].
- [61] J. W. Cronin, H. J. Frisch, M. J. Shochet, J. P. Boymond, R. Mermod, P. A. Piroue, and R. L. Sumner, “Production of hadrons with large transverse momentum at 200, 300, and 400 GeV”, *Phys. Rev. D* **11** (1975) 3105–3123.
- [62] **ALICE** Collaboration, S. Acharya *et al.*, “ $K^*(892)^0$ and $\phi(1020)$ production in p–Pb collisions at $\sqrt{s_{NN}} = 8.16$ TeV”, *Phys. Rev. C* **107** (2023) 055201, arXiv:2110.10042 [nucl-ex].

A The ALICE Collaboration

S. Acharya ¹²⁷, D. Adamová ⁸⁶, G. Aglieri Rinella ³³, M. Agnello ³⁰, N. Agrawal ⁵², Z. Ahammed ¹³⁵, S. Ahmad ¹⁶, S.U. Ahn ⁷², I. Ahuja ³⁸, A. Akhmedov ¹⁴¹, M. Al-Turany ⁹⁷, D. Aleksandrov ¹⁴¹, B. Alessandro ⁵⁷, H.M. Alfanda ⁶, R. Alfaro Molina ⁶⁸, B. Ali ¹⁶, A. Alici ²⁶, N. Alizadehvandchali ¹¹⁶, A. Alkin ³³, J. Alme ²¹, G. Alocco ⁵³, T. Alt ⁶⁵, A.R. Altamura ⁵¹, I. Altsybeev ⁹⁵, J.R. Alvarado ⁴⁵, M.N. Anaam ⁶, C. Andrei ⁴⁶, N. Andreou ¹¹⁵, A. Andronic ¹²⁶, E. Andronov ¹⁴¹, V. Anguelov ⁹⁴, F. Antinori ⁵⁵, P. Antonioli ⁵², N. Apadula ⁷⁴, L. Aphecetche ¹⁰³, H. Appelshäuser ⁶⁵, C. Arata ⁷³, S. Arcelli ²⁶, M. Aresti ²³, R. Arnaldi ⁵⁷, J.G.M.C.A. Arneiro ¹¹⁰, I.C. Arsene ²⁰, M. Arslandok ¹³⁸, A. Augustinus ³³, R. Averbeck ⁹⁷, M.D. Azmi ¹⁶, H. Baba ¹²⁴, A. Badalà ⁵⁴, J. Bae ¹⁰⁴, Y.W. Baek ⁴¹, X. Bai ¹²⁰, R. Bailhache ⁶⁵, Y. Bailung ⁴⁹, R. Bala ⁹¹, A. Balbino ³⁰, A. Baldisseri ¹³⁰, B. Balis ², D. Banerjee ⁴, Z. Banoo ⁹¹, F. Barile ³², L. Barioglio ⁹⁵, M. Barlou ⁷⁸, B. Barman ⁴², G.G. Barnaföldi ⁴⁷, L.S. Barnby ⁸⁵, E. Barreau ¹⁰³, V. Barret ¹²⁷, L. Barreto ¹¹⁰, C. Bartels ¹¹⁹, K. Barth ³³, E. Bartsch ⁶⁵, N. Bastid ¹²⁷, S. Basu ⁷⁵, G. Batigne ¹⁰³, D. Battistini ⁹⁵, B. Batyunya ¹⁴², D. Bauri ⁴⁸, J.L. Bazo Alba ¹⁰¹, I.G. Bearden ⁸³, C. Beattie ¹³⁸, P. Becht ⁹⁷, D. Behera ⁴⁹, I. Belikov ¹²⁹, A.D.C. Bell Hechavarria ¹²⁶, F. Bellini ²⁶, R. Bellwied ¹¹⁶, S. Belokurova ¹⁴¹, L.G.E. Beltran ¹⁰⁹, Y.A.V. Beltran ⁴⁵, G. Bencedi ⁴⁷, S. Beole ²⁵, Y. Berdnikov ¹⁴¹, A. Berdnikova ⁹⁴, L. Bergmann ⁹⁴, M.G. Besoiu ⁶⁴, L. Betev ³³, P.P. Bhaduri ¹³⁵, A. Bhasin ⁹¹, M.A. Bhat ⁴, B. Bhattacharjee ⁴², L. Bianchi ²⁵, N. Bianchi ⁵⁰, J. Bielčik ³⁶, J. Bielčiková ⁸⁶, A.P. Bigot ¹²⁹, A. Bilandzic ⁹⁵, G. Biro ⁴⁷, S. Biswas ⁴, N. Bize ¹⁰³, J.T. Blair ¹⁰⁸, D. Blau ¹⁴¹, M.B. Blidaru ⁹⁷, N. Bluhme ³⁹, C. Blume ⁶⁵, G. Boca ^{22,56}, F. Bock ⁸⁷, T. Bodova ²¹, S. Boi ²³, J. Bok ¹⁷, L. Boldizsár ⁴⁷, M. Bombara ³⁸, P.M. Bond ³³, G. Bonomi ^{134,56}, H. Borel ¹³⁰, A. Borissov ¹⁴¹, A.G. Borquez Carcamo ⁹⁴, H. Bossi ¹³⁸, E. Botta ²⁵, Y.E.M. Bouziani ⁶⁵, L. Bratrud ⁶⁵, P. Braun-Munzinger ⁹⁷, M. Bregant ¹¹⁰, M. Broz ³⁶, G.E. Bruno ^{96,32}, M.D. Buckland ²⁴, D. Budnikov ¹⁴¹, H. Buesching ⁶⁵, S. Bufalino ³⁰, P. Buhler ¹⁰², N. Burmasov ¹⁴¹, Z. Buthelezi ^{69,123}, A. Bylinkin ²¹, S.A. Bysiak ¹⁰⁷, J.C. Cabanillas Noris ¹⁰⁹, M. Cai ⁶, H. Caines ¹³⁸, A. Caliva ²⁹, E. Calvo Villar ¹⁰¹, J.M.M. Camacho ¹⁰⁹, P. Camerini ²⁴, F.D.M. Canedo ¹¹⁰, S.L. Cantway ¹³⁸, M. Carabas ¹¹³, A.A. Carballo ³³, F. Carnesecchi ³³, R. Caron ¹²⁸, L.A.D. Carvalho ¹¹⁰, J. Castillo Castellanos ¹³⁰, F. Catalano ^{33,25}, C. Ceballos Sanchez ¹⁴², I. Chakaberia ⁷⁴, P. Chakraborty ⁴⁸, S. Chandra ¹³⁵, S. Chapeland ³³, M. Chartier ¹¹⁹, S. Chattopadhyay ¹³⁵, S. Chattopadhyay ⁹⁹, T. Cheng ^{97,6}, C. Cheshkov ¹²⁸, B. Cheynis ¹²⁸, V. Chibante Barroso ³³, D.D. Chinellato ¹¹¹, E.S. Chizzali ^{11,95}, J. Cho ⁵⁹, S. Cho ⁵⁹, P. Chochula ³³, D. Choudhury ⁴², P. Christakoglou ⁸⁴, C.H. Christensen ⁸³, P. Christiansen ⁷⁵, T. Chujo ¹²⁵, M. Ciaccio ³⁰, C. Cicalo ⁵³, M.R. Ciupek ⁹⁷, G. Clai ^{III,52}, F. Colamaria ⁵¹, J.S. Colburn ¹⁰⁰, D. Colella ^{96,32}, M. Colocci ²⁶, M. Concas ^{IV,33}, G. Conesa Balbastre ⁷³, Z. Conesa del Valle ¹³¹, G. Contin ²⁴, J.G. Contreras ³⁶, M.L. Coquet ¹³⁰, P. Cortese ^{133,57}, M.R. Cosentino ¹¹², F. Costa ³³, S. Costanza ^{22,56}, C. Cot ¹³¹, J. Crkovská ⁹⁴, P. Crochet ¹²⁷, R. Cruz-Torres ⁷⁴, P. Cui ⁶, A. Dainese ⁵⁵, M.C. Danisch ⁹⁴, A. Danu ⁶⁴, P. Das ⁸⁰, P. Das ⁴, S. Das ⁴, A.R. Dash ¹²⁶, S. Dash ⁴⁸, A. De Caro ²⁹, G. de Cataldo ⁵¹, J. de Cuveland ³⁹, A. De Falco ²³, D. De Gruttola ²⁹, N. De Marco ⁵⁷, C. De Martin ²⁴, S. De Pasquale ²⁹, R. Deb ¹³⁴, R. Del Grande ⁹⁵, L. Dello Stritto ^{33,29}, W. Deng ⁶, P. Dhankher ¹⁹, D. Di Bari ³², A. Di Mauro ³³, B. Diab ¹³⁰, R.A. Diaz ^{142,7}, T. Dietel ¹¹⁴, Y. Ding ⁶, J. Ditzel ⁶⁵, R. Divià ³³, D.U. Dixit ¹⁹, Ø. Djuvsland ²¹, U. Dmitrieva ¹⁴¹, A. Dobrin ⁶⁴, B. Dönigus ⁶⁵, J.M. Dubinski ¹³⁶, A. Dubla ⁹⁷, S. Dudi ⁹⁰, P. Dupieux ¹²⁷, M. Durkac ¹⁰⁶, N. Dzalaiova ¹³, T.M. Eder ¹²⁶, R.J. Ehlers ⁷⁴, F. Eisenhut ⁶⁵, R. Ejima ⁹², D. Elia ⁵¹, B. Erazmus ¹⁰³, F. Ercolessi ²⁶, B. Espagnon ¹³¹, G. Eulisse ³³, D. Evans ¹⁰⁰, S. Evdokimov ¹⁴¹, L. Fabbietti ⁹⁵, M. Faggin ²⁸, J. Faivre ⁷³, F. Fan ⁶, W. Fan ⁷⁴, A. Fantoni ⁵⁰, M. Fasel ⁸⁷, A. Feliciello ⁵⁷, G. Feofilov ¹⁴¹, A. Fernández Téllez ⁴⁵, L. Ferrandi ¹¹⁰, M.B. Ferrer ³³, A. Ferrero ¹³⁰, C. Ferrero ⁵⁷, A. Ferretti ²⁵, V.J.G. Feuillard ⁹⁴, V. Filova ³⁶, D. Finogeev ¹⁴¹, F.M. Fionda ⁵³, E. Flatland ³³, F. Flor ¹¹⁶, A.N. Flores ¹⁰⁸, S. Foertsch ⁶⁹, I. Fokin ⁹⁴, S. Fokin ¹⁴¹, E. Fragiaco ⁵⁸, E. Frajna ⁴⁷, U. Fuchs ³³, N. Funicello ²⁹, C. Furget ⁷³, A. Furs ¹⁴¹, T. Fusayasu ⁹⁸, J.J. Gaardhøje ⁸³, M. Gagliardi ²⁵, A.M. Gago ¹⁰¹, T. Gahlaut ¹⁰⁹, C.D. Galvan ¹⁰⁹, D.R. Gangadharan ¹¹⁶, P. Ganoti ⁷⁸, C. Garabatos ⁹⁷, A.T. Garcia ¹³¹, T. García Chávez ⁴⁵, E. Garcia-Solis ⁹, C. Gargiulo ³³, P. Gasik ⁹⁷, A. Gautam ¹¹⁸, M.B. Gay Ducati ⁶⁷, M. Germain ¹⁰³, A. Ghimouz ¹²⁵, C. Ghosh ¹³⁵, M. Giacalone ⁵², G. Gioachin ³⁰, P. Giubellino ^{97,57}, P. Giubilato ²⁸, A.M.C. Glaenger ¹³⁰, P. Gläsel ⁹⁴, E. Glimos ¹²², D.J.Q. Goh ⁷⁶, V. Gonzalez ¹³⁷, P. Gordeev ¹⁴¹, M. Gorgon ², K. Goswami ⁴⁹, S. Gotovac ³⁴, V. Grabski ⁶⁸, L.K. Graczykowski ¹³⁶, E. Grecka ⁸⁶, A. Grelli ⁶⁰, C. Grigoras ³³, V. Grigoriev ¹⁴¹, S. Grigoryan ^{142,1}, F. Grosa ³³, J.F. Grosse-Oetringhaus ³³, R. Grosso ⁹⁷, D. Grund ³⁶, N.A. Grunwald ⁹⁴, G.G. Guardiani ¹¹¹, R. Guernane ⁷³, M. Guilbaud ¹⁰³, K. Gulbrandsen ⁸³, T. Gündem ⁶⁵, T. Gunji ¹²⁴,

W. Guo⁶, A. Gupta⁹¹, R. Gupta⁹¹, R. Gupta⁴⁹, K. Gwizdziel¹³⁶, L. Gyulai⁴⁷, C. Hadjidakis¹³¹, F.U. Haider⁹¹, S. Haidlova³⁶, M. Haldar⁴, H. Hamagaki⁷⁶, A. Hamdi⁷⁴, Y. Han¹³⁹, B.G. Hanley¹³⁷, R. Hannigan¹⁰⁸, J. Hansen⁷⁵, J.W. Harris¹³⁸, A. Harton⁹, M.V. Hartung⁶⁵, H. Hassan¹¹⁷, D. Hatzifotiadou⁵², P. Hauer⁴³, L.B. Havener¹³⁸, E. Hellbär⁹⁷, H. Helstrup³⁵, M. Hemmer⁶⁵, T. Herman³⁶, G. Herrera Corral⁸, F. Herrmann¹²⁶, S. Herrmann¹²⁸, K.F. Hetland³⁵, B. Heybeck⁶⁵, H. Hillemanns³³, B. Hippolyte¹²⁹, F.W. Hoffmann⁷¹, B. Hofman⁶⁰, G.H. Hong¹³⁹, M. Horst⁹⁵, A. Horzyk², Y. Hou⁶, P. Hristov³³, C. Hughes¹²², P. Huhn⁶⁵, L.M. Huhta¹¹⁷, T.J. Humanic⁸⁸, A. Hutson¹¹⁶, D. Hutter³⁹, M.C. Hwang¹⁹, R. Ilkaev¹⁴¹, H. Ilyas¹⁴, M. Inaba¹²⁵, G.M. Innocenti³³, M. Ippolitov¹⁴¹, A. Isakov⁸⁴, T. Isidori¹¹⁸, M.S. Islam⁹⁹, M. Ivanov⁹⁷, M. Ivanov¹³, V. Ivanov¹⁴¹, K.E. Iversen⁷⁵, M. Jablonski², B. Jacak^{19,74}, N. Jacazio²⁶, P.M. Jacobs⁷⁴, S. Jadlovská¹⁰⁶, J. Jadlovsky¹⁰⁶, S. Jaelani⁸², C. Jahnke¹¹⁰, M.J. Jakubowska¹³⁶, M.A. Janik¹³⁶, T. Janson⁷¹, S. Ji¹⁷, S. Jia¹⁰, A.A.P. Jimenez⁶⁶, F. Jonas^{74,87,126}, D.M. Jones¹¹⁹, J.M. Jowett^{33,97}, J. Jung⁶⁵, M. Jung⁶⁵, A. Junique³³, A. Jusko¹⁰⁰, M.J. Kabus^{33,136}, J. Kaewjai¹⁰⁵, P. Kalinak⁶¹, A.S. Kalteyer⁹⁷, A. Kalweit³³, D. Karatovic⁸⁹, O. Karavichev¹⁴¹, T. Karavicheva¹⁴¹, P. Karczmarczyk¹³⁶, E. Karpechev¹⁴¹, U. Kebschull⁷¹, R. Keidel¹⁴⁰, D.L.D. Keijdener⁶⁰, M. Keil³³, B. Ketzer⁴³, S.S. Khade⁴⁹, A.M. Khan¹²⁰, S. Khan¹⁶, A. Khanzadeev¹⁴¹, Y. Kharlov¹⁴¹, A. Khatun¹¹⁸, A. Khuntia³⁶, Z. Khuranova⁶⁵, B. Kileng³⁵, B. Kim¹⁰⁴, C. Kim¹⁷, D.J. Kim¹¹⁷, E.J. Kim⁷⁰, J. Kim¹³⁹, J. Kim⁵⁹, J. Kim⁷⁰, M. Kim¹⁹, S. Kim¹⁸, T. Kim¹³⁹, K. Kimura⁹², S. Kirsch⁶⁵, I. Kisel³⁹, S. Kiselev¹⁴¹, A. Kisiel¹³⁶, J.P. Kitowski², J.L. Klay⁵, J. Klein³³, S. Klein⁷⁴, C. Klein-Bösing¹²⁶, M. Kleiner⁶⁵, T. Klemenz⁹⁵, A. Kluge³³, C. Kobdaj¹⁰⁵, T. Kollegger⁹⁷, A. Kondratyev¹⁴², N. Kondratyeva¹⁴¹, J. Konig⁶⁵, S.A. Konigstorfer⁹⁵, P.J. Konopka³³, G. Kornakov¹³⁶, M. Korwieser⁹⁵, S.D. Koryciak², A. Kotliarov⁸⁶, N. Kovacic⁸⁹, V. Kovalenko¹⁴¹, M. Kowalski¹⁰⁷, V. Kozuharov³⁷, I. Králik⁶¹, A. Kravčáková³⁸, L. Krcal^{33,39}, M. Krivda^{100,61}, F. Krizek⁸⁶, K. Krizkova Gajdosova³³, M. Kroesen⁹⁴, M. Krüger⁶⁵, D.M. Krupova³⁶, E. Kryshen¹⁴¹, V. Kučera⁵⁹, C. Kuhn¹²⁹, P.G. Kuijer⁸⁴, T. Kumaoka¹²⁵, D. Kumar¹³⁵, L. Kumar⁹⁰, N. Kumar⁹⁰, S. Kumar³², S. Kundu³³, P. Kurashvili⁷⁹, A. Kurepin¹⁴¹, A.B. Kurepin¹⁴¹, A. Kuryakin¹⁴¹, S. Kushpil⁸⁶, V. Kuskov¹⁴¹, M. Kutyla¹³⁶, M.J. Kweon⁵⁹, Y. Kwon¹³⁹, S.L. La Pointe³⁹, P. La Rocca²⁷, A. Lakrathok¹⁰⁵, M. Lamanna³³, A.R. Landou⁷³, R. Langoy¹²¹, P. Larionov³³, E. Laudi³³, L. Lautner^{33,95}, R. Lavicka¹⁰², R. Lea^{134,56}, H. Lee¹⁰⁴, I. Legrand⁴⁶, G. Legras¹²⁶, J. Lehrbach³⁹, T.M. Lelek², R.C. Lemmon⁸⁵, I. León Monzón¹⁰⁹, M.M. Lesch⁹⁵, E.D. Lesser¹⁹, P. Lévai⁴⁷, X. Li¹⁰, B.E. Liang-gilman¹⁹, J. Lien¹²¹, R. Lietava¹⁰⁰, I. Likmeta¹¹⁶, B. Lim²⁵, S.H. Lim¹⁷, V. Lindenstruth³⁹, A. Lindner⁴⁶, C. Lippmann⁹⁷, D.H. Liu⁶, J. Liu¹¹⁹, G.S.S. Liveraro¹¹¹, I.M. Lofnes²¹, C. Loizides⁸⁷, S. Lokos¹⁰⁷, J. Lomker⁶⁰, P. Loncar³⁴, X. Lopez¹²⁷, E. López Torres⁷, P. Lu^{97,120}, F.V. Lugo⁶⁸, J.R. Luhder¹²⁶, M. Lunardon²⁸, G. Luparello⁵⁸, Y.G. Ma⁴⁰, M. Mager³³, A. Maire¹²⁹, E.M. Majerz², M.V. Makariev³⁷, M. Malaev¹⁴¹, G. Malfattore²⁶, N.M. Malik⁹¹, Q.W. Malik²⁰, S.K. Malik⁹¹, L. Malinina^{I,VII,142}, D. Mallick¹³¹, N. Mallick⁴⁹, G. Mandaglio^{31,54}, S.K. Mandal⁷⁹, V. Manko¹⁴¹, F. Manso¹²⁷, V. Manzari⁵¹, Y. Mao⁶, R.W. Marcjan², G.V. Margagliotti²⁴, A. Margotti⁵², A. Marín⁹⁷, C. Markert¹⁰⁸, P. Martinengo³³, M.I. Martínez⁴⁵, G. Martínez García¹⁰³, M.P.P. Martins¹¹⁰, S. Masciocchi⁹⁷, M. Masera²⁵, A. Masoni⁵³, L. Massacrier¹³¹, O. Massen⁶⁰, A. Mastroserio^{132,51}, O. Matonoha⁷⁵, S. Mattiazzo²⁸, A. Matyja¹⁰⁷, C. Mayer¹⁰⁷, A.L. Mazuecos³³, F. Mazzaschi²⁵, M. Mazzilli³³, J.E. Mdhuli¹²³, Y. Melikyan⁴⁴, A. Menchaca-Rocha⁶⁸, J.E.M. Mendez⁶⁶, E. Meninno¹⁰², A.S. Menon¹¹⁶, M. Meres¹³, Y. Miake¹²⁵, L. Micheletti³³, D.L. Mihaylov⁹⁵, K. Mikhaylov^{142,141}, D. Miśkowiec⁹⁷, A. Modak⁴, B. Mohanty⁸⁰, M. Mohisin Khan^{V,16}, M.A. Molander⁴⁴, S. Monira¹³⁶, C. Mordasini¹¹⁷, D.A. Moreira De Godoy¹²⁶, I. Morozov¹⁴¹, A. Morsch³³, T. Mrnjavac³³, V. Muccifora⁵⁰, S. Muhuri¹³⁵, J.D. Mulligan⁷⁴, A. Mulliri²³, M.G. Munhoz¹¹⁰, R.H. Munzer⁶⁵, H. Murakami¹²⁴, S. Murray¹¹⁴, L. Musa³³, J. Musinsky⁶¹, J.W. Myrcha¹³⁶, B. Naik¹²³, A.I. Nambrath¹⁹, B.K. Nandi⁴⁸, R. Nania⁵², E. Nappi⁵¹, A.F. Nassirpour¹⁸, A. Nath⁹⁴, C. Nattrass¹²², M.N. Naydenov³⁷, A. Neagu²⁰, A. Negru¹¹³, E. Nekrasova¹⁴¹, L. Nellen⁶⁶, R. Nepeivoda⁷⁵, S. Nese²⁰, G. Neskovic³⁹, N. Nicassio⁵¹, B.S. Nielsen⁸³, E.G. Nielsen⁸³, S. Nikolaev¹⁴¹, S. Nikulin¹⁴¹, V. Nikulin¹⁴¹, F. Noferini⁵², S. Noh¹², P. Nomokonov¹⁴², J. Norman¹¹⁹, N. Novitzky⁸⁷, P. Nowakowski¹³⁶, A. Nyanin¹⁴¹, J. Nystrand²¹, S. Oh¹⁸, A. Ohlson⁷⁵, V.A. Okorokov¹⁴¹, J. Oleniacz¹³⁶, A. Onnerstad¹¹⁷, C. Oppedisano⁵⁷, A. Ortiz Velasquez⁶⁶, J. Otwinowski¹⁰⁷, M. Oya⁹², K. Oyama⁷⁶, Y. Pachmayer⁹⁴, S. Padhan⁴⁸, D. Pagano^{134,56}, G. Paic⁶⁶, S. Paisano-Guzmán⁴⁵, A. Palasciano⁵¹, S. Panebianco¹³⁰, H. Park¹²⁵, H. Park¹⁰⁴, J. Park⁵⁹, J.E. Parkkila³³, Y. Patley⁴⁸, B. Paul²³, M.M.D.M. Paulino¹¹⁰,

H. Pei⁶, T. Peitzmann⁶⁰, X. Peng¹¹, M. Pennisi²⁵, S. Perciballi²⁵, D. Peresunko¹⁴¹, G.M. Perez⁷,
 Y. Pestov¹⁴¹, V. Petrov¹⁴¹, M. Petrovici⁴⁶, R.P. Pezzi^{103,67}, S. Piano⁵⁸, M. Pikna¹³, P. Pillot¹⁰³,
 O. Pinazza^{52,33}, L. Pinsky¹¹⁶, C. Pinto⁹⁵, S. Pisano⁵⁰, M. Płoskoń⁷⁴, M. Planinic⁸⁹, F. Pliquett⁶⁵,
 M.G. Poghosyan⁸⁷, B. Polichtchouk¹⁴¹, S. Politano³⁰, N. Poljak⁸⁹, A. Pop⁴⁶,
 S. Porteboeuf-Houssais¹²⁷, V. Pozdniakov¹⁴², I.Y. Pozos⁴⁵, K.K. Pradhan⁴⁹, S.K. Prasad⁴,
 S. Prasad⁴⁹, R. Preghenella⁵², F. Prino⁵⁷, C.A. Pruneau¹³⁷, I. Pshenichnov¹⁴¹, M. Puccio³³,
 S. Pucillo²⁵, Z. Pugelova¹⁰⁶, S. Qiu⁸⁴, L. Quaglia²⁵, S. Ragoni¹⁵, A. Rai¹³⁸,
 A. Rakotozafindrabe¹³⁰, L. Ramello^{133,57}, F. Rami¹²⁹, T.A. Rancien⁷³, M. Rasa²⁷, S.S. Räsänen⁴⁴,
 R. Rath⁵², M.P. Rauch²¹, I. Ravasenga³³, K.F. Read^{87,122}, C. Reckziegel¹¹², A.R. Redelbach³⁹,
 K. Redlich^{VI,79}, C.A. Reetz⁹⁷, H.D. Regules-Medel⁴⁵, A. Rehman²¹, F. Reidt³³, H.A. Reme-Ness³⁵,
 Z. Rescakova³⁸, K. Reygers⁹⁴, A. Riabov¹⁴¹, V. Riabov¹⁴¹, R. Ricci²⁹, M. Richter²⁰,
 A.A. Riedel⁹⁵, W. Riegler³³, A.G. Riffero²⁵, C. Ristea⁶⁴, M.V. Rodriguez³³, M. Rodríguez
 Cahuantzi⁴⁵, S.A. Rodríguez Ramírez⁴⁵, K. Røed²⁰, R. Rogalev¹⁴¹, E. Rogochaya¹⁴²,
 T.S. Rogoschinski⁶⁵, D. Rohr³³, D. Röhrich²¹, P.F. Rojas⁴⁵, S. Rojas Torres³⁶, P.S. Rokita¹³⁶,
 G. Romanenko²⁶, F. Ronchetti⁵⁰, A. Rosano^{31,54}, E.D. Rosas⁶⁶, K. Roslon¹³⁶, A. Rossi⁵⁵,
 A. Roy⁴⁹, S. Roy⁴⁸, N. Rubini²⁶, D. Ruggiano¹³⁶, R. Rui²⁴, P.G. Russek², R. Russo⁸⁴,
 A. Rustamov⁸¹, E. Ryabinkin¹⁴¹, Y. Ryabov¹⁴¹, A. Rybicki¹⁰⁷, H. Rytönen¹¹⁷, J. Ryu¹⁷,
 W. Rzesza¹³⁶, O.A.M. Saarimäki⁴⁴, S. Sadhu³², S. Sadosky¹⁴¹, J. Saetre²¹, K. Šafařík³⁶, P. Saha⁴²,
 S.K. Saha⁴, S. Saha⁸⁰, B. Sahoo⁴⁸, B. Sahoo⁴⁹, R. Sahoo⁴⁹, S. Sahoo⁶², D. Sahu⁴⁹, P.K. Sahu⁶²,
 J. Saini¹³⁵, K. Sajdakova³⁸, S. Sakai¹²⁵, M.P. Salvan⁹⁷, S. Sambyal⁹¹, D. Samitz¹⁰², I. Sanna^{33,95},
 T.B. Saramela¹¹⁰, D. Sarkar⁸³, P. Sarma⁴², V. Sarritzu²³, V.M. Sarti⁹⁵, M.H.P. Sas³³, S. Sawan⁸⁰,
 E. Scapparone⁵², J. Schambach⁸⁷, H.S. Scheid⁶⁵, C. Schiaua⁴⁶, R. Schicker⁹⁴, F. Schlepfer⁹⁴,
 A. Schmah⁹⁷, C. Schmidt⁹⁷, H.R. Schmidt⁹³, M.O. Schmidt³³, M. Schmidt⁹³, N.V. Schmidt⁸⁷,
 A.R. Schmier¹²², R. Schotter¹²⁹, A. Schröter³⁹, J. Schukraft³³, K. Schweda⁹⁷, G. Scioli²⁶,
 E. Scomparin⁵⁷, J.E. Seger¹⁵, Y. Sekiguchi¹²⁴, D. Sekihata¹²⁴, M. Selina⁸⁴, I. Selyuzhenkov⁹⁷,
 S. Senyukov¹²⁹, J.J. Seo⁹⁴, D. Serebryakov¹⁴¹, L. Serkin⁶⁶, L. Šerkšnytė⁹⁵, A. Sevcenco⁶⁴,
 T.J. Shaba⁶⁹, A. Shabetai¹⁰³, R. Shahoyan³³, A. Shangaraev¹⁴¹, B. Sharma⁹¹, D. Sharma⁴⁸,
 H. Sharma⁵⁵, M. Sharma⁹¹, S. Sharma⁷⁶, S. Sharma⁹¹, U. Sharma⁹¹, A. Shatat¹³¹, O. Sheibani¹¹⁶,
 K. Shigaki⁹², M. Shimomura⁷⁷, J. Shin¹², S. Shirinkin¹⁴¹, Q. Shou⁴⁰, Y. Sibiriak¹⁴¹, S. Siddhanta⁵³,
 T. Siemiarczuk⁷⁹, T.F. Silva¹¹⁰, D. Silvermyr⁷⁵, T. Simantathammakul¹⁰⁵, R. Simeonov³⁷, B. Singh⁹¹,
 B. Singh⁹⁵, K. Singh⁴⁹, R. Singh⁸⁰, R. Singh⁹¹, R. Singh⁴⁹, S. Singh¹⁶, V.K. Singh¹³⁵,
 V. Singhal¹³⁵, T. Sinha⁹⁹, B. Sitar¹³, M. Sitta^{133,57}, T.B. Skaali²⁰, G. Skorodumovs⁹⁴,
 M. Slupecki⁴⁴, N. Smirnov¹³⁸, R.J.M. Snellings⁶⁰, E.H. Solheim²⁰, J. Song¹⁷, C. Sonnabend^{33,97},
 J.M. Sonneveld⁸⁴, F. Soramel²⁸, A.B. Soto-herandez⁸⁸, R. Spijkers⁸⁴, I. Sputowska¹⁰⁷, J. Staa⁷⁵,
 J. Stachel⁹⁴, I. Stan⁶⁴, P.J. Steffanic¹²², S.F. Stiefelmaier⁹⁴, D. Stocco¹⁰³, I. Storehaug²⁰,
 P. Stratmann¹²⁶, S. Strazzi²⁶, A. Sturmiolo^{31,54}, C.P. Stylianidis⁸⁴, A.A.P. Suaide¹¹⁰, C. Suire¹³¹,
 M. Sukhanov¹⁴¹, M. Suljic³³, R. Sultanov¹⁴¹, V. Sumberia⁹¹, S. Sumowidagdo⁸², I. Szarka¹³,
 M. Szymkowski¹³⁶, S.F. Taghavi⁹⁵, G. Taillepied⁹⁷, J. Takahashi¹¹¹, G.J. Tambave⁸⁰, S. Tang⁶,
 Z. Tang¹²⁰, J.D. Tapia Takaki¹¹⁸, N. Tapus¹¹³, L.A. Tarasovicova¹²⁶, M.G. Tarzila⁴⁶, G.F. Tassielli³²,
 A. Tauro³³, G. Tejeda Muñoz⁴⁵, A. Telesca³³, L. Terlizzi²⁵, C. Terrevoli¹¹⁶, S. Thakur⁴,
 D. Thomas¹⁰⁸, A. Tikhonov¹⁴¹, N. Tiltmann¹²⁶, A.R. Timmins¹¹⁶, M. Tkacik¹⁰⁶, T. Tkacik¹⁰⁶,
 A. Toia⁶⁵, R. Tokumoto⁹², K. Tomohiro⁹², N. Topilskaya¹⁴¹, M. Toppi⁵⁰, T. Tork¹³¹, P.V. Torres⁶⁶,
 V.V. Torres¹⁰³, A.G. Torres Ramos³², A. Trifiro^{31,54}, A.S. Triolo^{33,31,54}, S. Tripathy⁵²,
 T. Tripathy⁴⁸, S. Trogolo³³, V. Trubnikov³, W.H. Trzaska¹¹⁷, T.P. Trzcinski¹³⁶, A. Tumkin¹⁴¹,
 R. Turrisi⁵⁵, T.S. Tveter²⁰, K. Ullaland²¹, B. Ulukutlu⁹⁵, A. Uras¹²⁸, M. Urioni¹³⁴, G.L. Usai²³,
 M. Vala³⁸, N. Valle²², L.V.R. van Doremalen⁶⁰, M. van Leeuwen⁸⁴, C.A. van Veen⁹⁴, R.J.G. van
 Weelden⁸⁴, P. Vande Vyvre³³, D. Varga⁴⁷, Z. Varga⁴⁷, M. Vasileiou⁷⁸, A. Vasiliev¹⁴¹, O. Vázquez
 Doce⁵⁰, O. Vazquez Rueda¹¹⁶, V. Vechernin¹⁴¹, E. Vercellin²⁵, S. Vergara Limón⁴⁵, R. Verma⁴⁸,
 L. Vermunt⁹⁷, R. Vértesi⁴⁷, M. Verweij⁶⁰, L. Vickovic³⁴, Z. Vilakazi¹²³, O. Villalobos Baillie¹⁰⁰,
 A. Villani²⁴, A. Vinogradov¹⁴¹, T. Virgili²⁹, M.M.O. Virta¹¹⁷, V. Vislavicius⁷⁵, A. Vodopyanov¹⁴²,
 B. Volkel³³, M.A. Völkl⁹⁴, S.A. Voloshin¹³⁷, G. Volpe³², B. von Haller³³, I. Vorobyev³³,
 N. Vozniuk¹⁴¹, J. Vrláková³⁸, J. Wan⁴⁰, C. Wang⁴⁰, D. Wang⁴⁰, Y. Wang⁴⁰, Y. Wang⁶,
 A. Wegrzynek³³, F.T. Weiglhofer³⁹, S.C. Wenzel³³, J.P. Wessels¹²⁶, J. Wiechula⁶⁵, J. Wikne²⁰,
 G. Wilk⁷⁹, J. Wilkinson⁹⁷, G.A. Willems¹²⁶, B. Windelband⁹⁴, M. Winn¹³⁰, J.R. Wright¹⁰⁸,
 W. Wu⁴⁰, Y. Wu¹²⁰, R. Xu⁶, A. Yadav⁴³, A.K. Yadav¹³⁵, Y. Yamaguchi⁹², S. Yang²¹, S. Yano⁹²,
 E.R. Yeats¹⁹, Z. Yin⁶, I.-K. Yoo¹⁷, J.H. Yoon⁵⁹, H. Yu¹², S. Yuan²¹, A. Yuncu⁹⁴, V. Zaccolo²⁴,

C. Zampolli ³³, F. Zanone ⁹⁴, N. Zardoshti ³³, A. Zarochentsev ¹⁴¹, P. Závada ⁶³, N. Zaviyalov¹⁴¹, M. Zhalov ¹⁴¹, B. Zhang ⁶, C. Zhang ¹³⁰, L. Zhang ⁴⁰, S. Zhang ⁴⁰, X. Zhang ⁶, Y. Zhang¹²⁰, Z. Zhang ⁶, M. Zhao ¹⁰, V. Zhrebchevskii ¹⁴¹, Y. Zhi¹⁰, C. Zhong⁴⁰, D. Zhou ⁶, Y. Zhou ⁸³, J. Zhu ^{55,6}, Y. Zhu⁶, S.C. Zugravel ⁵⁷, N. Zurlo ^{134,56}

Affiliation Notes

^I Deceased

^{II} Also at: Max-Planck-Institut für Physik, Munich, Germany

^{III} Also at: Italian National Agency for New Technologies, Energy and Sustainable Economic Development (ENEA), Bologna, Italy

^{IV} Also at: Dipartimento DET del Politecnico di Torino, Turin, Italy

^V Also at: Department of Applied Physics, Aligarh Muslim University, Aligarh, India

^{VI} Also at: Institute of Theoretical Physics, University of Wrocław, Poland

^{VII} Also at: An institution covered by a cooperation agreement with CERN

Collaboration Institutes

¹ A.I. Alikhanyan National Science Laboratory (Yerevan Physics Institute) Foundation, Yerevan, Armenia

² AGH University of Krakow, Cracow, Poland

³ Bogolyubov Institute for Theoretical Physics, National Academy of Sciences of Ukraine, Kiev, Ukraine

⁴ Bose Institute, Department of Physics and Centre for Astroparticle Physics and Space Science (CAPSS), Kolkata, India

⁵ California Polytechnic State University, San Luis Obispo, California, United States

⁶ Central China Normal University, Wuhan, China

⁷ Centro de Aplicaciones Tecnológicas y Desarrollo Nuclear (CEADEN), Havana, Cuba

⁸ Centro de Investigación y de Estudios Avanzados (CINVESTAV), Mexico City and Mérida, Mexico

⁹ Chicago State University, Chicago, Illinois, United States

¹⁰ China Institute of Atomic Energy, Beijing, China

¹¹ China University of Geosciences, Wuhan, China

¹² Chungbuk National University, Cheongju, Republic of Korea

¹³ Comenius University Bratislava, Faculty of Mathematics, Physics and Informatics, Bratislava, Slovak Republic

¹⁴ COMSATS University Islamabad, Islamabad, Pakistan

¹⁵ Creighton University, Omaha, Nebraska, United States

¹⁶ Department of Physics, Aligarh Muslim University, Aligarh, India

¹⁷ Department of Physics, Pusan National University, Pusan, Republic of Korea

¹⁸ Department of Physics, Sejong University, Seoul, Republic of Korea

¹⁹ Department of Physics, University of California, Berkeley, California, United States

²⁰ Department of Physics, University of Oslo, Oslo, Norway

²¹ Department of Physics and Technology, University of Bergen, Bergen, Norway

²² Dipartimento di Fisica, Università di Pavia, Pavia, Italy

²³ Dipartimento di Fisica dell'Università and Sezione INFN, Cagliari, Italy

²⁴ Dipartimento di Fisica dell'Università and Sezione INFN, Trieste, Italy

²⁵ Dipartimento di Fisica dell'Università and Sezione INFN, Turin, Italy

²⁶ Dipartimento di Fisica e Astronomia dell'Università and Sezione INFN, Bologna, Italy

²⁷ Dipartimento di Fisica e Astronomia dell'Università and Sezione INFN, Catania, Italy

²⁸ Dipartimento di Fisica e Astronomia dell'Università and Sezione INFN, Padova, Italy

²⁹ Dipartimento di Fisica 'E.R. Caianiello' dell'Università and Gruppo Collegato INFN, Salerno, Italy

³⁰ Dipartimento DISAT del Politecnico and Sezione INFN, Turin, Italy

³¹ Dipartimento di Scienze MIFT, Università di Messina, Messina, Italy

³² Dipartimento Interateneo di Fisica 'M. Merlin' and Sezione INFN, Bari, Italy

³³ European Organization for Nuclear Research (CERN), Geneva, Switzerland

³⁴ Faculty of Electrical Engineering, Mechanical Engineering and Naval Architecture, University of Split, Split, Croatia

³⁵ Faculty of Engineering and Science, Western Norway University of Applied Sciences, Bergen, Norway

- ³⁶ Faculty of Nuclear Sciences and Physical Engineering, Czech Technical University in Prague, Prague, Czech Republic
- ³⁷ Faculty of Physics, Sofia University, Sofia, Bulgaria
- ³⁸ Faculty of Science, P.J. Šafárik University, Košice, Slovak Republic
- ³⁹ Frankfurt Institute for Advanced Studies, Johann Wolfgang Goethe-Universität Frankfurt, Frankfurt, Germany
- ⁴⁰ Fudan University, Shanghai, China
- ⁴¹ Gangneung-Wonju National University, Gangneung, Republic of Korea
- ⁴² Gauhati University, Department of Physics, Guwahati, India
- ⁴³ Helmholtz-Institut für Strahlen- und Kernphysik, Rheinische Friedrich-Wilhelms-Universität Bonn, Bonn, Germany
- ⁴⁴ Helsinki Institute of Physics (HIP), Helsinki, Finland
- ⁴⁵ High Energy Physics Group, Universidad Autónoma de Puebla, Puebla, Mexico
- ⁴⁶ Horia Hulubei National Institute of Physics and Nuclear Engineering, Bucharest, Romania
- ⁴⁷ HUN-REN Wigner Research Centre for Physics, Budapest, Hungary
- ⁴⁸ Indian Institute of Technology Bombay (IIT), Mumbai, India
- ⁴⁹ Indian Institute of Technology Indore, Indore, India
- ⁵⁰ INFN, Laboratori Nazionali di Frascati, Frascati, Italy
- ⁵¹ INFN, Sezione di Bari, Bari, Italy
- ⁵² INFN, Sezione di Bologna, Bologna, Italy
- ⁵³ INFN, Sezione di Cagliari, Cagliari, Italy
- ⁵⁴ INFN, Sezione di Catania, Catania, Italy
- ⁵⁵ INFN, Sezione di Padova, Padova, Italy
- ⁵⁶ INFN, Sezione di Pavia, Pavia, Italy
- ⁵⁷ INFN, Sezione di Torino, Turin, Italy
- ⁵⁸ INFN, Sezione di Trieste, Trieste, Italy
- ⁵⁹ Inha University, Incheon, Republic of Korea
- ⁶⁰ Institute for Gravitational and Subatomic Physics (GRASP), Utrecht University/Nikhef, Utrecht, Netherlands
- ⁶¹ Institute of Experimental Physics, Slovak Academy of Sciences, Košice, Slovak Republic
- ⁶² Institute of Physics, Homi Bhabha National Institute, Bhubaneswar, India
- ⁶³ Institute of Physics of the Czech Academy of Sciences, Prague, Czech Republic
- ⁶⁴ Institute of Space Science (ISS), Bucharest, Romania
- ⁶⁵ Institut für Kernphysik, Johann Wolfgang Goethe-Universität Frankfurt, Frankfurt, Germany
- ⁶⁶ Instituto de Ciencias Nucleares, Universidad Nacional Autónoma de México, Mexico City, Mexico
- ⁶⁷ Instituto de Física, Universidade Federal do Rio Grande do Sul (UFRGS), Porto Alegre, Brazil
- ⁶⁸ Instituto de Física, Universidad Nacional Autónoma de México, Mexico City, Mexico
- ⁶⁹ iThemba LABS, National Research Foundation, Somerset West, South Africa
- ⁷⁰ Jeonbuk National University, Jeonju, Republic of Korea
- ⁷¹ Johann-Wolfgang-Goethe Universität Frankfurt Institut für Informatik, Fachbereich Informatik und Mathematik, Frankfurt, Germany
- ⁷² Korea Institute of Science and Technology Information, Daejeon, Republic of Korea
- ⁷³ Laboratoire de Physique Subatomique et de Cosmologie, Université Grenoble-Alpes, CNRS-IN2P3, Grenoble, France
- ⁷⁴ Lawrence Berkeley National Laboratory, Berkeley, California, United States
- ⁷⁵ Lund University Department of Physics, Division of Particle Physics, Lund, Sweden
- ⁷⁶ Nagasaki Institute of Applied Science, Nagasaki, Japan
- ⁷⁷ Nara Women's University (NWU), Nara, Japan
- ⁷⁸ National and Kapodistrian University of Athens, School of Science, Department of Physics, Athens, Greece
- ⁷⁹ National Centre for Nuclear Research, Warsaw, Poland
- ⁸⁰ National Institute of Science Education and Research, Homi Bhabha National Institute, Jatni, India
- ⁸¹ National Nuclear Research Center, Baku, Azerbaijan
- ⁸² National Research and Innovation Agency - BRIN, Jakarta, Indonesia
- ⁸³ Niels Bohr Institute, University of Copenhagen, Copenhagen, Denmark
- ⁸⁴ Nikhef, National institute for subatomic physics, Amsterdam, Netherlands
- ⁸⁵ Nuclear Physics Group, STFC Daresbury Laboratory, Daresbury, United Kingdom
- ⁸⁶ Nuclear Physics Institute of the Czech Academy of Sciences, Husinec-Řež, Czech Republic
- ⁸⁷ Oak Ridge National Laboratory, Oak Ridge, Tennessee, United States

- 88 Ohio State University, Columbus, Ohio, United States
- 89 Physics department, Faculty of science, University of Zagreb, Zagreb, Croatia
- 90 Physics Department, Panjab University, Chandigarh, India
- 91 Physics Department, University of Jammu, Jammu, India
- 92 Physics Program and International Institute for Sustainability with Knotted Chiral Meta Matter (SKCM2), Hiroshima University, Hiroshima, Japan
- 93 Physikalisches Institut, Eberhard-Karls-Universität Tübingen, Tübingen, Germany
- 94 Physikalisches Institut, Ruprecht-Karls-Universität Heidelberg, Heidelberg, Germany
- 95 Physik Department, Technische Universität München, Munich, Germany
- 96 Politecnico di Bari and Sezione INFN, Bari, Italy
- 97 Research Division and ExtreMe Matter Institute EMMI, GSI Helmholtzzentrum für Schwerionenforschung GmbH, Darmstadt, Germany
- 98 Saga University, Saga, Japan
- 99 Saha Institute of Nuclear Physics, Homi Bhabha National Institute, Kolkata, India
- 100 School of Physics and Astronomy, University of Birmingham, Birmingham, United Kingdom
- 101 Sección Física, Departamento de Ciencias, Pontificia Universidad Católica del Perú, Lima, Peru
- 102 Stefan Meyer Institut für Subatomare Physik (SMI), Vienna, Austria
- 103 SUBATECH, IMT Atlantique, Nantes Université, CNRS-IN2P3, Nantes, France
- 104 Sungkyunkwan University, Suwon City, Republic of Korea
- 105 Suranaree University of Technology, Nakhon Ratchasima, Thailand
- 106 Technical University of Košice, Košice, Slovak Republic
- 107 The Henryk Niewodniczanski Institute of Nuclear Physics, Polish Academy of Sciences, Cracow, Poland
- 108 The University of Texas at Austin, Austin, Texas, United States
- 109 Universidad Autónoma de Sinaloa, Culiacán, Mexico
- 110 Universidade de São Paulo (USP), São Paulo, Brazil
- 111 Universidade Estadual de Campinas (UNICAMP), Campinas, Brazil
- 112 Universidade Federal do ABC, Santo Andre, Brazil
- 113 Universitatea Nationala de Stiinta si Tehnologie Politehnica Bucuresti, Bucharest, Romania
- 114 University of Cape Town, Cape Town, South Africa
- 115 University of Derby, Derby, United Kingdom
- 116 University of Houston, Houston, Texas, United States
- 117 University of Jyväskylä, Jyväskylä, Finland
- 118 University of Kansas, Lawrence, Kansas, United States
- 119 University of Liverpool, Liverpool, United Kingdom
- 120 University of Science and Technology of China, Hefei, China
- 121 University of South-Eastern Norway, Kongsberg, Norway
- 122 University of Tennessee, Knoxville, Tennessee, United States
- 123 University of the Witwatersrand, Johannesburg, South Africa
- 124 University of Tokyo, Tokyo, Japan
- 125 University of Tsukuba, Tsukuba, Japan
- 126 Universität Münster, Institut für Kernphysik, Münster, Germany
- 127 Université Clermont Auvergne, CNRS/IN2P3, LPC, Clermont-Ferrand, France
- 128 Université de Lyon, CNRS/IN2P3, Institut de Physique des 2 Infinis de Lyon, Lyon, France
- 129 Université de Strasbourg, CNRS, IPHC UMR 7178, F-67000 Strasbourg, France, Strasbourg, France
- 130 Université Paris-Saclay, Centre d'Etudes de Saclay (CEA), IRFU, Département de Physique Nucléaire (DPhN), Saclay, France
- 131 Université Paris-Saclay, CNRS/IN2P3, IJCLab, Orsay, France
- 132 Università degli Studi di Foggia, Foggia, Italy
- 133 Università del Piemonte Orientale, Vercelli, Italy
- 134 Università di Brescia, Brescia, Italy
- 135 Variable Energy Cyclotron Centre, Homi Bhabha National Institute, Kolkata, India
- 136 Warsaw University of Technology, Warsaw, Poland
- 137 Wayne State University, Detroit, Michigan, United States
- 138 Yale University, New Haven, Connecticut, United States
- 139 Yonsei University, Seoul, Republic of Korea
- 140 Zentrum für Technologie und Transfer (ZTT), Worms, Germany

¹⁴¹ Affiliated with an institute covered by a cooperation agreement with CERN

¹⁴² Affiliated with an international laboratory covered by a cooperation agreement with CERN.